Resistive Switching in Mott Insulators and Correlated Systems

*Etienne Janod, Julien Tranchant, Benoit Corraze, Madec Querré, Pablo Stoliar, Marcelo Rozenberg, Tristan Cren, Dimitri Roditchev, Vinh Ta Phuoc, Marie-Paule Besland, and Laurent Cario**

Resistive random access memories (ReRAM) form an emerging type of non-volatile memories, based on an electrically driven resistive switching (RS) of an active material. This Feature Article focuses on a broad class of ReRAM where the active material is a Mott insulator or a correlated system. These materials can indeed undergo various insulator-to-metal transitions (IMT) in response to external perturbations such as electronic doping or temperature. These IMT explain most of resistive switching observed in correlated insulators as, for example, the Joule heating induced RS in VO_2. The main part of this Feature Article is dedicated to a new mechanism of resistive switching recently unveiled in canonical Mott insulators such as $(V_{1-x}Cr_x)_2O_3$, $NiS_{2-x}Se_x$ and AM_4Q_8 (A = Ga, Ge; M = V, Nb, Ta, Mo; Q = S, Se, Te). In these narrow gap Mott insulators, an electronic avalanche breakdown induces a resistive switching, first volatile above a threshold electric field of a few kV/cm and then non-volatile at higher field. The low resistance state is related to the creation of granular conductive filaments, which, in the non-volatile case, can be erased by means of Joule heating. ReRAM devices based on this new type of out of equilibrium Mott insulator-to-metal transition display promising performances.

Dr. E. Janod, Dr. J. Tranchant, Dr. B. Corraze, M. Querré, Dr. M.-P. Besland, Dr. L. Cario
Institut des Matériaux Jean Rouxel (IMN)
Université de Nantes
CNRS, 2 rue de la Houssinière
BP 32229, 44322 Nantes Cedex 3, France
E-mail: Laurent.Cario@cnrs-imn.fr

Dr. P. Stoliar
CIC nanoGUNE
20018 Donostia – San Sebastian
Basque Country, Spain

Dr. M. Rozenberg
Laboratoire de Physique des Solides
CNRS-UMR8502
Université de Paris-Sud
Orsay 91405, France

Dr. T. Cren, Dr. D. Roditchev
Institut des Nanosciences de Paris
Université Pierre et Marie Curie
CNRS UMR 7588
4 place Jussieu, F-75005 Paris, France

Dr. V. Ta Phuoc
GREMAN, CNRS UMR 7347-CEA
Université F. Rabelais
UFR Sciences, Parc de Grandmont
37200 Tours, France

DOI: 10.1002/adfm.201500823

1. Introduction

The huge non-volatile memory market is led by the Flash technology used, for example, in Flash SD cards and solid state drives. However, the limit of this technology in downscaling will hinder its development in a near future.[1] Several emerging random access memories (RAM),[2] that is, phase-change RAM (PCRAM),[3] magnetic RAMs (MRAM),[4] and resistive RAM (ReRAM),[5] are currently considered as interesting candidates to overcome the shortcomings of Flash memories. However, ReRAMs appear as a very appealing solution among these potential candidates, thanks to a very simple architecture and promizing memory performances.[1] ReRAMs are hence envisioned to replace the Flash technology in mass storage applications before 2020.[6] In ReRAM information storage is enabled by a non-volatile and reversible switching between two different resistance states of an active material. This resistive switching is obtained by applying short electric pulses to the active material most of the time sandwiched between two metallic electrodes. A large variety of materials are known to exhibit a reversible electric-pulse-induced resistive switching phenomenon, such as transition metal oxides Band Insulators (TiO_2, $SrTiO_3$, $SrZrO_3$, etc.) or copper and silver based chalcogenides.[7–11] So far, different mechanisms based on thermochemical or electrochemical effects have been proposed to explain the non-volatile resistive switching observed in these materials.[5,7,9] But resistive switching is also observed in Mott insulators that form a large class of materials particularly attractive in the context of memory applications.[11] They can indeed undergo various kinds of insulator-to-metal transitions (IMT) in response to different external perturbations like pressure, temperature, and electronic filling. These IMT are often associated with huge modifications of the electrical resistance and therefore allows generating high and low resistance states, that is, the two logical states ('0' and '1') of a ReRAM device.

This Feature Article focuses on this particularly interesting class of ReRAM in which the active material is a Mott Insulator. Section 2 describes briefly the theoretical background of Mott insulators, and the different ways to break the Mott insulating

state to induce IMT in these systems. Most resistive switching in Mott insulators are closely related to these IMT that can be induced by electric pulses either thanks to Joule heating, or by means of electrochemical or thermochemical mechanisms. Section 3 gives an overview of resistive switching in Mott insulators and correlated insulators based on these known mechanisms first evidenced in band insulators or amorphous insulators. Conversely, a new mechanism of resistive switching was recently discovered in Mott insulators.[12–14] This Feature Article focuses particularly on this new type of resistive switching which is triggered by an electric field induced avalanche breakdown ultimately leading to a non volatile electronic phase separation at the nanoscale. Sections 4 and 5 describe, respectively, the volatile avalanche breakdown phenomenon and its non volatile consequences in Mott insulators. Section 6 displays the potential of this universal property of narrow gap Mott insulators for ReRAM applications. Finally, this Feature Article proposes a classification of resistive switching mechanisms in Mott insulators based on the types of insulator-to-metal transition and controlling parameters involved in the resistive switching.

2. Mott Insulators and Mott Insulator to Metal Transitions

2.1. Basic Concepts

Unlike conventional band insulators and semiconductors, Mott insulators contain unpaired electrons in their ground state. However, a drastic condition is required to bring up the Mott insulating state: an electronic filling exactly equal to an integer number of unpaired electron per site.[15] According to conventional band theories, such compounds with an odd number of electrons should be metallic since their Fermi levels lie in the middle of a band, as shown in **Figure 1**a.

However, even in absence of disorder, many of these materials are actually insulators. The discrepancy comes from a crucial parameter incorrectly described in conventional band theories, the on-site Coulombian repulsion. For simplicity, let's consider the situation of a single band system that is half-filled (i.e., with one electron per site). Thus, if the Coulomb repulsion (Hubbard) energy U exceeds the bandwidth W, the half-filled band splits into two sub-bands, the lower (LHB) and upper (UHB) Hubbard bands (see Figure 1a). Thanks to the U term, a Mott-Hubbard gap E_G opens up between the LHB and the UHB if U is larger than the bandwidth W, roughly equal to $E_G \approx U - W$. The theoretical description of the Mott insulating state has been a long-standing problem[16–18] and only modern approaches such as the dynamical mean field theory (DMFT) have successfully predicted the whole phase diagram of this class of materials.[19,20] A salient feature of this universal k_BT/W versu U/W phase diagram[19–22] is the first order (Mott) transition line which separates a metallic domain at low U/W from a paramagnetic Mott insulator (PMI) domain for $U/W > 1.15$,[23] as depicted in Figure 1a. This Mott metal-insulator transition line terminates at a second order critical endpoint at high temperature for $T_{endpoint} \approx 0.025\,W/k_B$.[19,22] This endpoint has an interesting fundamental consequence: the absence of crystallographic symmetry breaking across the

Etienne Janod completed his Ph.D. at CEA Grenoble in 1996 on cuprates superconductors. After a postdoc at University of California San Diego, he joined CNRS and integrated the Institut des Matériaux Jean Rouxel (IMN) in Nantes, France, with a research project focused on quantum magnetism. With B. Corraze and L. Cario, he engaged in 2005 an activity devoted to unconventional electronic properties of correlated compounds. He is currently working on strongly correlated systems out-of-equilibrium, from a fundamental point of view and also for applications in information storage and neurocomputing.

Benoit Corraze completed his Ph.D. on cuprates superconductors at the Laboratoire de Physique des Solides (LPS) of Orsay, France in 1991. He was then appointed associated professor at the University of Nantes. He joined the Institut des Matériaux Jean Rouxel (IMN) in Nantes, France where he developed a research activity on electronic transport phenomena focusing on non linear behavior. With E. Janod and L. Cario, he built up a research program devoted to strongly correlated systems, especially on unconventional properties and functionalities emerging under electric field.

Laurent Cario, received his Ph.D. in physical chemistry at the University of Nantes, France, in 1998. He worked subsequently during two years at the department of chemistry of Cornell University (USA) until he was appointed CNRS research associate at the Institut des Matériaux Jean Rouxel (IMN) in Nantes (France). In 2014 he was promoted CNRS research director. He is a specialist of the physical chemistry of chalcogenide compounds. With B. Corraze and E. Janod, he is currently leading the research program on correlated oxide and chalcogenide compounds at IMN including the work on resistive switching in narrow gap Mott insulators.

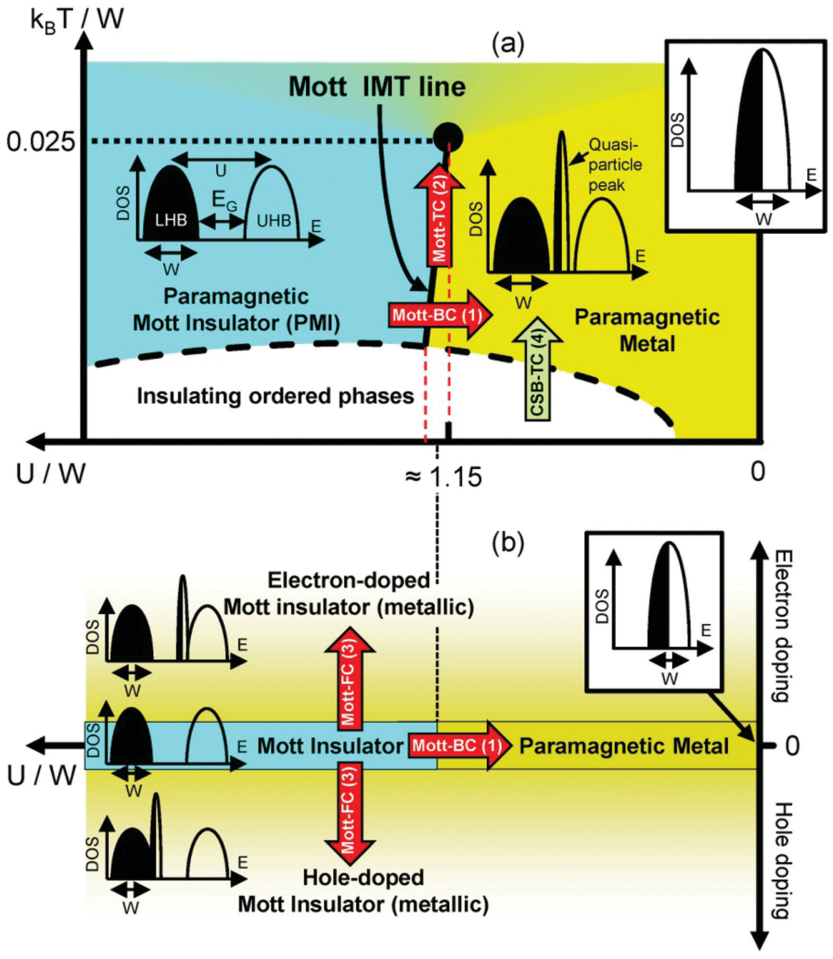

Figure 1. a) Schematic phase diagram of two- and three-dimensional half-filled compounds undergoing a Mott insulator-to-metal transition, displayed as k_BT/W versus U/W. T, U, and W are the temperature, the Hubbard electron-electron repulsion term and the bandwidth, respectively. Typical electronic Density of States (DOS) are displayed in relevant regions of the phase diagram : in absence of electron correlation ($U/W = 0$), in the correlated metal domain slightly below $U/W = 1.15$ and in the Mott insulating state for $U/W > 1.15$. b) Diagram of doped Mott insulators, represented as electron and hole doping away from half-filling vs correlation strength U/W, for intermediate temperature $T_{ordered\ phase} < T < T_{endpoint}$ shown in part (a). Red arrows indicate the universal IMT that emerge from the Paramagnetic Mott Insulator state, that is, the "type 1" Mott,bandwith controlled (Mott-BC), and the "type 2" Mott, temperature controlled (Mott-TC) transitions crossing the Mott line in half-filled compounds, as well as the "type 3" filling-controlled (Mott-FC) IMT. The green arrow corresponds to a non-universal "type 4" Temperature-Controlled insulator-to-metal transition towards a long range order insulating state, associated in real systems to a Crystallographic Symmetry Breaking (CSB-TC).

Mott line, since one can connect continuously the PMI and metallic phases shown in Figure 1a through a high temperature path above the endpoint. Another major contribution of the DMFT is to predict a specific signature of electronic correlation close to the Mott IMT line: while a gap between the lower and upper Hubbard bands exists on the insulating side, a quasiparticle peak develops in the gap at the Fermi energy on the metallic side (see Figure 1a).[19] Whereas the Mott line and the high temperature part of the phase diagram are universal, the low temperature part is material-dependent and can present various kinds of long-range (for example magnetic or orbital) orders.

Beyond the particular case of half-filling, Figure 1b presents a generalized phase diagram at any electronic filling, represented as x (hole or electron doping level away from half-filling) versus U/W.[24] This diagram reveals that the Mott insulating state is stable only at half-filling and that doped Mott insulators are metallic. Both phase diagrams highlight the three IMT, represented by red arrows in Figure 1, that emerge from the Mott insulating state:[24]

1) Bandwidth controlled IMT. This IMT, noted "type 1" thereafter, corresponds to the crossing of the Mott transition line (see Figure 1a) induced by tuning the correlation strength U/W,[24–27] This can be achieved by applying an external pressure which enhances the orbitals overlaps and increases thus the bandwidth W;
2) Temperature controlled IMT. This IMT, noted "type 2" thereafter, is driven by temperature and also relies on the crossing of the Mott line in a narrow window of U/W around ≈ 1.15, between the red dotted line in Figure 1a. This IMT occurs between a low temperature metal and a high temperature insulator,[28] which strongly contrasts with the more usual transitions from a low-T insulator to a high-T metal,
3) Filling controlled IMT.[24] This IMT, noted "type 3" thereafter, occurs when the band filling deviates from half filling (see Figure 1b). This may be achieved by tuning the electronic filling thanks to chemical doping.

Several interesting conclusions can be inferred from these phase diagrams of correlated compounds. Figure 1a indeed shows that a canonical paramagnetic Mott insulator (PMI) can not present an insulator-to-metal transition by increasing temperature.[29] However, temperature-controlled insulator to metal transitions are possible in half-filled correlated systems if they exhibit a long-range (e.g., magnetic or orbital) order at low temperature, as shown by the green arrow in Figure 1a. In real systems, such Temperature Controlled IMT involve a symmetry breaking, which is in general a crystallographic symmetry breaking. These insulator-to-metal transitions, noted "type 4" thereafter, strongly differ from the three Mott IMT discussed above which occur without crystallographic symmetry breaking. In the compounds showing a "type 4" temperature controlled IMT involving a crystallographic symmetry breaking, the driving force behind the IMT is not related only to the U versus W competition, but necessarily includes an additional mechanism.

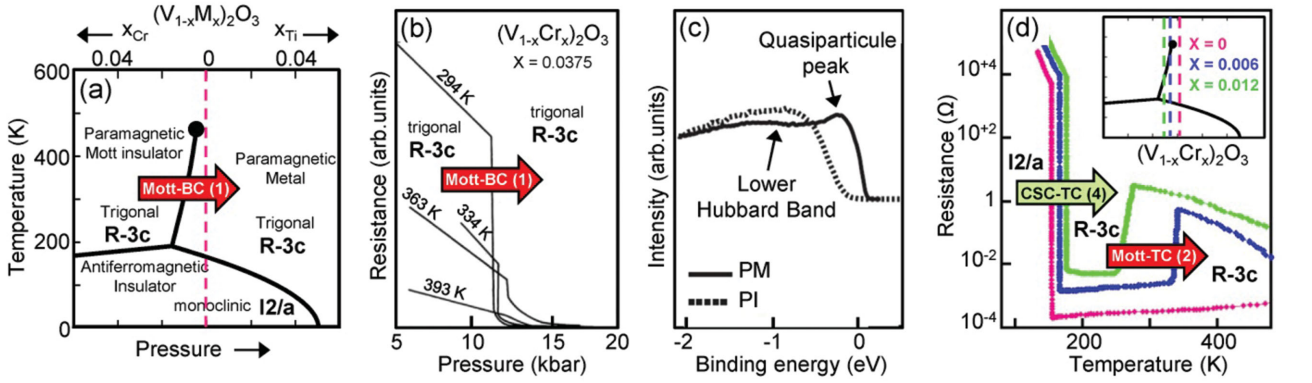

Figure 2. a) Phase diagram of $(V_{1-x}M_x)_2O_3$, with M = Cr and Ti. In this system, changing the *V*/*M* ratio by 1% is equivalent to applying an external pressure of ≈ 4 kbar.[32] b) Resistance versus pressure across the Mott insulator-to-metal transition in $(V_{0.9625}Cr_{0.0375})_2O_3$. Adapted with permission.[33] Copyright 1970, American Physical Society. c) Photoemission spectra taken at 300 K (in the Paramagnetic Mott Insulator state, PI) and 200 K (Paramagnetic Metal state, PM) from the (001) surface of $(V_{0.989}Cr_{0.011})_2O_3$. The black arrows highlight the Lower Hubbard Band in the PI state, on top of which a quasiparticle peak appears in the PM state. Adapted with permission.[34] Copyright 2009, American Physical Society. d) Resistivity vs temperature in pure V_2O_3 and $(V_{1-x}Cr_x)_2O_3$ with $x = 0.006$ and 0.012. Adapted with permission.[28] Copyright 1980, American Physical Society.

2.2. Examples of Canonical Mott Insulators

The phase diagrams shown in Figure 1 are purely theoretical and an important issue is to establish their relevance in real compounds. The most famous "canonical" Mott insulator is probably the oxide compound $(V_{1-x}Cr_x)_2O_3$. Its phase diagram[30–32] shown in **Figure 2**a indeed compares very well with theoretical predictions. It contains a Mott IMT line ending around 450 K and separating a Mott insulating phase from a metallic phase. Figure 2b shows that applying a moderate pressure increases the bandwidth[25] and induces a type 1 (Mott) bandwidth-controlled IMT in $(V_{0.9625}Cr_{0.0375})_2O_3$.[33] Moreover, despite the strong decrease of unit cell volume at the IMT indicating a first order transition, the IMT occurs between two R-3c phases, that is, without any crystallographic symmetry breaking.[32] Also, the observation of a quasiparticle peak above the lower Hubbard band, shown in Figure 2c, confirms the correlated nature of the metallic state in pure V_2O_3.[34] Finally, pure and Cr-substituted V_2O_3 display an antiferromagnetic insulating (AFI) phase at low temperature; in pure V_2O_3, an IMT occurs between the AFI (space group I2/*a*) and the metallic phase (space group R-3c) at ≈165 K.[35] According to the classification proposed in Section 2.1, this transition does not correspond to a Mott transition. It corresponds to a "type 4" IMT, that is, a transition associated with a crystallographic symmetry breaking and driven by an additional mechanism which is magnetic ordering in this case. Figure 2d shows that two successive transitions (type 4, AFI → metal and type 2, metal → PMI) appear in a narrow V/Cr substitution level around 1%.[28] The type 2 low temperature metal to high temperature paramagnetic insulator is expected from the theoretical phase diagram of Figure 1a, as the Mott IMT line is not vertical but slightly tilted.[19,21,22] All these features indicate that the V_2O_3 system is a prototypical Mott insulator.

Beyond the V_2O_3 system, a few other canonical Mott insulators have been identified, such as the 2D molecular family κ-$(BEDT\text{-}TTF)_2X$[36] or the chalcogenide system $NiS_{2-x}Se_x$.[37] Recently another series of chalcogenides, the AM_4Q_8 compounds (A = Ga, Ge; M = V, Nb, Ta, Mo; Q = S, Se, Te), has emerged as a potential new example of canonical Mott insulator. These compounds exhibit a lacunar spinel structure, in which the electronic sites correspond to the tetrahedral transition metal clusters M_4 shown in the inset of **Figure 3**a.[38] In GaM_4Q_8 compounds, each M_4 cluster contain one unpaired electron among seven (M = V, Nb, Ta) or eleven (M = Mo) *d* electrons.[39] These compounds own a narrow gap of 0.1–0.3 eV, which can be tuned by chemical substitution.[40] At ambient pressure, all AM_4Q_8 compounds display two important characteristics of canonical Mott insulators: they are paramagnetic insulators above 55K[39,41,42] and do not exhibit any temperature-controlled IMT up to 800 K, as shown in Figure 3-a. Moreover, these compounds exhibit a bandwidth-controlled IMT (type 1). $GaTa_4Se_8$ and $GaNb_4Q_8$ (Q = S, Se) undergo indeed an insulator-to-metal transition under pressure, with superconductivity at $T_C \approx 2$–7 K in the pressurized metallic state above 11 GPa.[43,44] Recent studies of transport properties under pressure in $GaTa_4Se_8$, shown in Figure 3b, prove that this pressure-induced (bandwidth-controlled) IMT is of first order with an hysteresis, as expected from LDA+DMFT calculations.[45,46] Moreover, the optical conductivity shown on Figure 3c reveals the signature of a quasi-particle peak in the pressurized metallic phase of $GaTa_4Se_8$.[47] Another interesting feature of AM_4Q_8 is that they undergo filling-controlled IMT (type 3) when doped on the A site or on the M site.[48] All these results demonstrate that the AM_4Q_8 compounds display the expected characteristics of a canonical Mott insulator.

2.3. Insulator-to-Metal Transition in Other Correlated Insulators

Beyond the examples of canonical Mott insulators and Mott IMT, many other half-filled insulators display temperature-controlled IMT potentially interesting for memory applications. Most of these IMT are clearly not of the Mott type 1, 2, or 3 discussed above, but belongs to the type 4 IMT

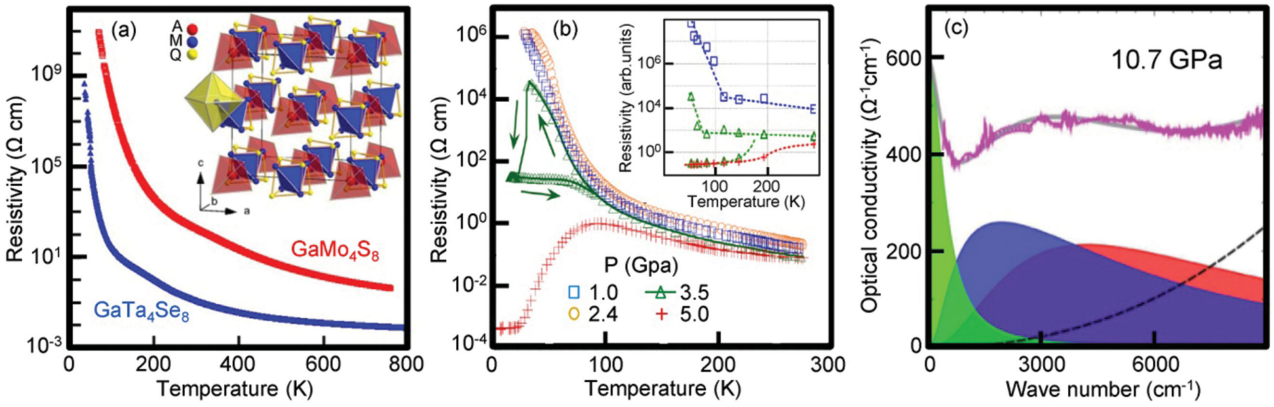

Figure 3. a) Resistivity versus temperature up to 800 K in two representative AM_4Q_8 compounds, $GaMo_4S_8$ and $GaTa_4Se_8$. Inset : crystallographic structure of AM_4Q_8 (A = Ga, Ge; M = V, Nb, Ta, Mo; Q = S, Se) compounds, highlighting the M_4 tetrahedral clusters. b) Resistivity vs temperature (4 K ≤ T ≤ 300 K) at different pressures in $GaTa_4Se_8$ in the PMI (1 and 2.4 GPa) and metallic (5 GPa) states. The "bistability" of resistivity at 3.5 GPa is a clear indication of the phase coexistence close to the Mott IMT line. Inset: LDA + DMFT results for the resistivity as a function of the temperature. The red crosses, blue squares, and green triangles correspond to the metal, insulator and coexistent solutions, respectively. The lines are a guide for the eyes. Reproduced with permission.[45] Copyright 2014, American Physical Society. c) Optical conductivity vs wave number in $GaTa_4Se_8$ in the metallic state appearing beyond the Mott line under pressure (10.7 GPa). The low energy contribution corresponds to the quasiparticle peak, a typical signature of electronic correlation. Reproduced with permission.[47] Copyright 2013, American Physical Society.

since they are associated with crystallographic symmetry breakings. **Figure 4** gathers several examples of such "type 4" insulator-to-metal transitions, which include IMT in Ca_2RuO_4 (T_{IMT} = 357 K),[49] VO_2 (T_{IMT} = 340 K),[50] NbO_2 (T_{IMT} = 1070 K),[51] and $ANiO_3$ perovskites.[52,53] As illustrated by the representative example of VO_2 shown in **Figure 5**, the temperature-pressure phase diagram of these half-filled insulators contains, unlike canonical systems (see Figure 1a and Figure 2a), an IMT line separating a low-T insulating phase from a high-T metallic phase of different crystallographic symmetry.[54,55]

Finally it is worth mentioning that temperature controlled IMT can also happen in non-half-filled correlated systems. In mixed valence systems, insulator-to-metal transition may indeed go along with a charge ordering transition, as observed, for example, in 2D molecular systems[56] and in transition metal oxides (a short review can be found in the literature).[57] Such IMT are always accompanied by crystallographic symmetry breaking, with a lower symmetry in the charge ordered insulating phase at low temperature. They are thus related with the temperature-controlled IMT (type 4) of half-filled systems discussed above. A prominent example is

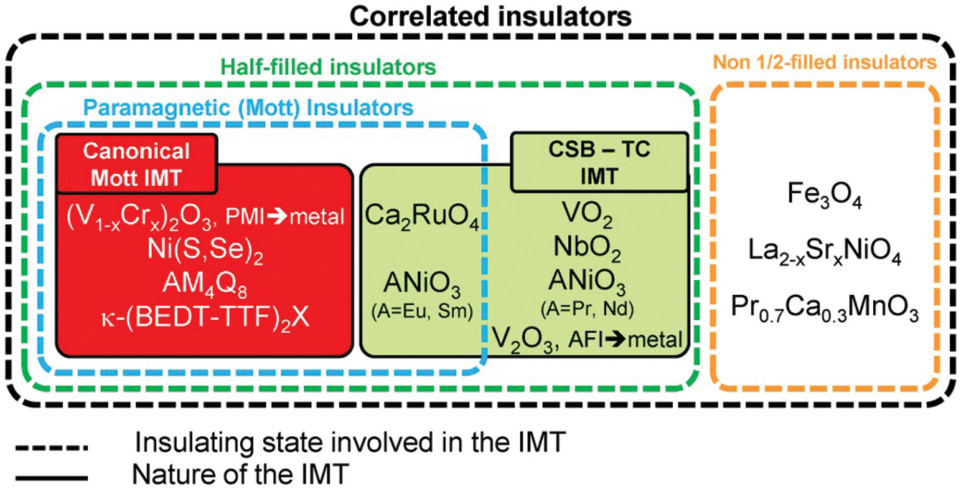

Figure 4. Classification of IMT occuring in various correlated insulators of interest for resistive switching effects. Unlike canonical (Mott) IMT which result only from a competition between U and W (IMT in $(V_{1-x}Cr_x)_2O_3$, $Ni(S,Se)_2$, AM_4Q_8 and κ(BEDT-TTF)$_2$X), Temperature-Controlled IMT associated with a Crystallographic Symmetry Breaking (CSB-TC) are driven by another mechanism : Jahn-Teller effect at T_{IMT} = 357 K in Ca_2RuO_4,[49] a Peierls-Mott instability at T_{IMT} = 340 K in VO_2[50] and at T_{IMT} = 1070K in NbO_2,[51] magnetic ordering at T_{IMT} = 165 K in pure V_2O_3[35] or a complex site-selective transition in $ANiO_3$ perovskites.[52] The compounds gathered on the right hand side are typical examples of non-half-filled systems where the insulating state results from a charge ordering.

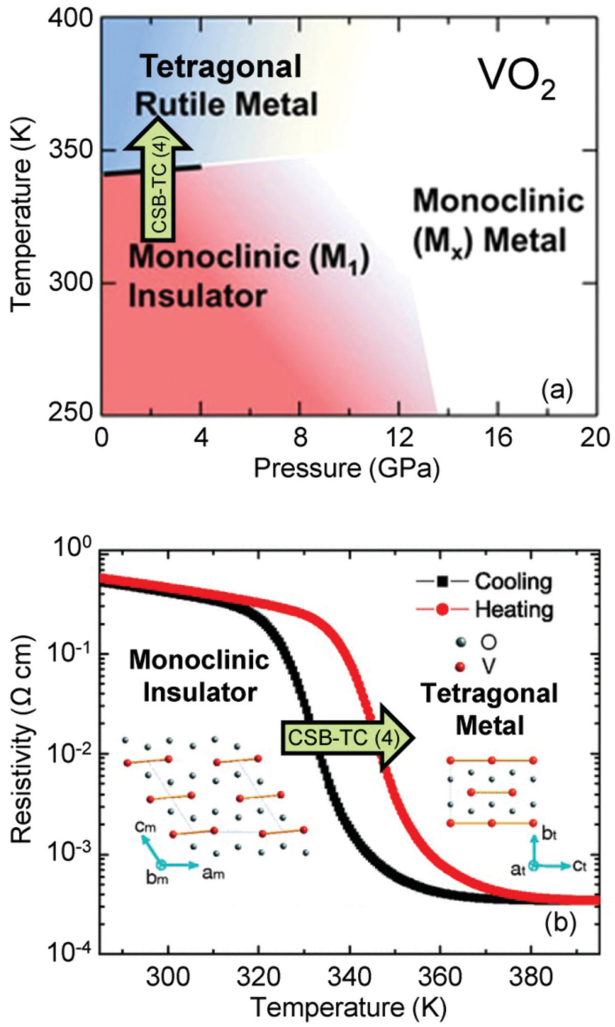

Figure 5. a) Temperature-pressure phase diagram of VO_2. Adapted with permission.[54] Copyright 2014, American Institute of Physics. b) Resistivity versus temperature at the "type 4" IMT in VO_2. This IMT is associated with a crystallographic symmetry breaking between the monoclinic low-*T* and the tetragonal high-*T* phases. Reproduced with permission.[55] Copyright 2013, American Physical Society.

the Verwey transition occurring at 122 K in the magnetite Fe_3O_4.[58]

3. Resistive Switching in Correlated Insulators

3.1. Resistive Switching Related to Temperature-Controlled Insulator-to-Metal Transitions

In Section 2, two different classes of thermally driven IMT were introduced, occurring with (type 4 IMT) or without (type 2 IMT) crystallographic symmetry breaking. For both types of IMT, temperature can be used as a tuning parameter triggering a resistive switching. Indeed, the application of an electric field at $T < T_{IMT}$ can lead to Joule self-heating and therefore to a strong modification of resistance if the sample temperature exceeds T_{IMT}.

Such a thermal mechanism is at play in correlated metal in the close vicinity of the Mott line, as recently confirmed by a DMFT theoretical study.[59] In compounds such as $(V_{1-x}Cr_x)_2O_3$ ($x \approx 0.01$)[60] and $NiS_{2-x}Se_x$ ($x \approx 0.45$),[61,62] a volatile resistive switching under electric field indeed occurs due to Joule heating effects, between a low *T* metallic phase and a high *T* paramagnetic Mott insulator phase (see Figure 2a). A more recent work on $GaTa_4Se_8$ under pressure also underlines the important role of Joule heating near the Mott IMT line.[45] This switching are related to a Mott type 2 IMT and leads to an increase of resistance during the pulse.

Also, this thermal mechanism convincingly explains the switchings observed in the compounds displaying a type 4 IMT, such as in VO_2,[63,64] NbO_2,[65] Ca_2RuO_4,[5,66] in pure V_2O_3 below the AFI–metal transition temperature[67–69] and in magnetite Fe_3O_4.[70,71] These thermally induced switchings are essentially volatile (i.e., low resistance state is maintained only under electric field) and appears above a threshold voltage corresponding to a Joule heating threshold. The materials showing such a volatile threshold switching behavior[72] can be used as selectors in Resistive Random Access Memory (ReRAM) crossbar arrays, in order to suppress the undesired sneak currents (a general introduction on this concept can be found in the literature).[73] However, non-volatile resistive switching (i.e., the low resistance state remains even after the end of electric pulses) can be also achieved in these correlated insulators by fine tuning the working temperature within the hysteresis domain of the first order IMT, as demonstrated in VO_2.[74,75] However this compound was barely studied in the context of ReRAM applications.

3.2. Valence Change Memories (VCM) with Mott Insulators

Resistive switching based on valence change is one of the most known mechanisms for ReRAM, and has been the focus of many reviews.[5,7–11] In non-stoichiometric transition metal oxides like $SrTiO_{3-x}$, TiO_{2-x}, HfO_{2-x}, Ta_2O_{5-x}, the migration of oxygen vacancies under electric field along grain boundaries or dislocations induces a valence change of the cations in the vicinity of theses defects.

At the local scale, a transition occurs between a band insulator involving empty *d*-orbitals (d^0) with cations in their high valence state (e.g., Ti^{4+}) to a metallic state (degenerated doped insulator) involving partially filled *d*-orbitals ($d^{+\delta}$) with cations in a lower valence state (e.g., Ti^{3+}). In oxides like $SrTiO_{3-x}$, TiO_{2-x}, HfO_{2-x}, Ta_2O_{5-x}, this phenomenon leads to a reversible bipolar resistive switching[76] by the formation/destruction of a metallic filamentary path between the electrodes.[5,9,77] Alternatively, the electro-migration phenomenon can also occur close to the metallic electrode/insulator oxide interface and lead to a bipolar resistive switching by modification of a Schottky barrier.[5,8] This interface type VCM was for example observed for $SrRuO_3/SrTi_{0.99}Nb_{0.01}O_3$/Ag junction.[8,78]

As discussed in Section 2.1, filling controlled insulator-to-metal transition can also occur in Mott insulators. In oxide Mott insulators this type of IMT is easily achieved by tuning the oxygen content.[24] For this reason, non-stoichiometric oxide Mott insulators can exhibit both filamentary and interfacial VCM type resistive switching. Interfacial VCM type resistive

switching was observed for various Mott or correlated transition metal oxides such as La_2CuO_4,[8] $Pr_{0.7}Ca_{0.3}MnO_3$,[79,80] and $YBa_2Cu_3O_{7-x}$.[81] On the other hand, filamentary VCM type resistive switching was reported in many transition metal oxide Mott insulators.[11,82] This type of resistive switching was observed for example in NiO,[83,84] CuO,[85,86] and CoO,[87] and proposed in Fe_2O_3,[88] and MnO_x.[89] The most studied system is by far NiO. In this compound, many studies have revealed that the resistive switching is related to the creation of metallic Ni filaments by a thermally assisted ionic migration process while the destruction of these filaments occurs due to Joule heating. As a consequence unipolar resistive switching[76] was mainly reported for NiO.[10,83,84] In the same way, resistive switching in CuO films was associated to the formation and destruction of conducting filaments made of a reduced phase, namely Cu_2O.[85] Conversely, resistive switching in CoO films was proposed to be related to the formation of an oxidized phase Co_3O_4.[89]

3.3. Resistive Switching Induced by Dielectric Breakdown

As discussed in the previous sections, most of the resistive transitions observed in Mott and correlated insulators can be explained by Joule heating driven phase transition leading to an IMT, or by a filling controlled IMT induced by ionic migration. However several experimental reports of resistive switching in Mott insulators or correlated systems cannot be explained by these mechanisms. This is the case of the volatile resistive switching reported in the quasi-one-dimensional Mott insulators Sr_2CuO_3 and $SrCuO_2$ by Taguchi et al.[90] or in the insulating charge-ordered state of $La_{2-x}Sr_xNiO_4$.[91] A so called dielectric breakdown occurs for these compounds above a threshold field of the order of 10^2–10^4 V/cm. Similar phenomena were also reported for the family of chalcogenide Mott insulators AM_4Q_8 (A = Ga, Ge; M = V, Nb, Ta, Mo; Q = S, Se),[12,13] or for the molecular Mott insulators K-TCNQ,[92] and κ-(BEDT-TTF)$_2$Cu[N(CN)$_2$]Br.[93] In that context, many theoretical works were recently devoted to dielectric breakdown caused by strong electric fields in Mott insulators. These studies have mainly focused on the Zener breakdown for Mott insulators.[94,97] For instance, calculations were performed in 1D Hubbard chains using exact diagonalization,[94] and time-dependent density matrix renormalization group,[95] or in the limit of large dimensions using dynamical mean field theory.[96] All these theoretical studies have predicted non-linear behavior in the current–voltage characteristics, and the existence of a threshold field (E_{th}) beyond which a field induced metal appears. This dielectric breakdown should occur when the electric field is such that it bends the Hubbard bands by the gap energy E_G within the length ξ of the order of to the unit cell. Hence, the Zener breakdown is predicted to occur for strength of the electric field $E_{th} \sim E_G/\xi$ of the order of 10^6–10^7 V/cm.[94] This is at least two orders of magnitude larger than the values observed experimentally.[13,90,91,93] As a consequence, volatile resistive switching in Mott insulators cannot be explained by a Zener breakdown scenario. Alternatively, recent studies on the AM_4Q_8 Mott insulators support that the dielectric breakdown originates from an electric field induced electronic avalanche phenomenon. The following sections will describe in more detail the experimental evidences, theoretical modeling and ReRAM applications of this universal property of Mott Insulators.

4. Electric Field Induced Dielectric Breakdown in Mott Insulators

4.1. Avalanche Breakdown in AM_4Q_8 Narrow Gap Mott Insulators

AM_4Q_8 (A = Ga, Ge; M = V, Nb, Ta, Mo; Q = S, Se) Mott insulators are very sensitive to electric pulses.[12,13,98,99] When an electric field pulse exceeding a threshold field (E_{th}) of a few kV/cm is applied to these compounds they undergo a sudden decrease of their resistance. As an example **Figure 6** shows the typical time evolution of the intensity $I(t)$ and of the voltage $V_{sample}(t)$ across a GaV_4S_8 crystal during the application of a series of short voltage pulses to a circuit composed of the crystal connected in series with a load resistance (sketched in Figure 6a).[100] An abrupt increase of the intensity and a lowering of the voltage across the sample is observed for applied voltages that exceed the threshold voltage V_{th} (or more precisely the threshold field $E_{th} = V_{th}/d$ with d the inter-electrodes distance) shown as red dotted line in Figure 6b. These transitions correspond to volatile resistive switchings from a high to a low resistance state, since resistance returns to its initial value after the electric pulse terminates. It is worth noting that these transitions cannot be explained by a temperature controlled IMT (described as type 2 IMT in Part 3.1) since AM_4Q_8 compounds do not present any IMT in temperature (see Figure 3a). Moreover simple estimates using the energy release during the pulse and the activated temperature dependence of the resistivity show that Joule heating cannot account for the abrupt resistive switching.[13] Figure 6 shows that the resistive switching occurs only above a threshold electric field E_{th} (≈ 7 kV/cm for GaV_4S_8) and after a time t_{delay} which decreases as the voltage across the sample increases. The sample voltage V_{sample} after the resistive switching event always lies on the same value $V_{th} \approx 12$ V (or $E_{th} \approx 7$ kV/cm) that also corresponds to the lower voltage that can induce a resistive switch in DC measurements. The AM_4Q_8 compounds exhibit therefore a very specific current–voltage characteristics with two branches. The first one corresponds to the non transited state and follows the Ohm's law. The second branch, which is almost vertical and lies at the threshold field, corresponds to the "transited" state (see red dotted line in Figure 6c). All AM_4Q_8 compounds exhibit the same type of $I(V)$ characteristic with threshold electric field in the 1–10 kV/cm range.[13] The magnitude of the threshold field in AM_4Q_8 Mott insulators as well as their $I(V)$ characteristics compare well with the threshold field values and $I(V)$ characteristics observed for avalanche breakdowns in narrow gap semiconductors.[101] For this reason it was proposed that the resistive switching observed in the Mott Insulators AM_4Q_8 originates from an avalanche breakdown phenomenon.[102] In semiconductors the avalanche threshold field varies as a power law of the band gap and follows the universal law $E_{th} \propto E_G^{2.5}$.[103,104] Figure 6d reveals that AM_4Q_8 compounds have a similar variation of the threshold field as a function of the Mott-Hubbard gap.[102] This power law

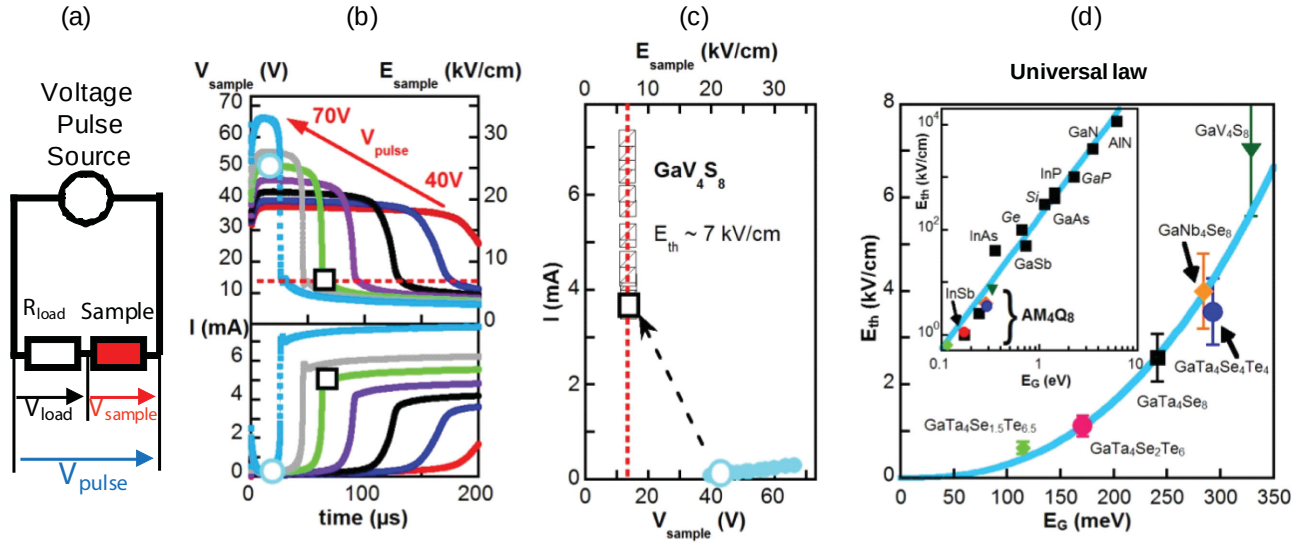

Figure 6. a) Example of circuit used for measurement. b) Time dependence of the voltage and intensity across a GaV_4S_8 single crystal during 200 µs pulses for several voltages applied to the circuit. Above a threshold voltage of ≈12 V (equivalent to 7 kV/cm), a resistive switching occurs after a time t_{delay} which decreases when the sample voltage (electric field) increases. All the transitions observed during the pulses are volatile, that is, the resistance is the same before and after the electric pulse. c) Current–voltage characteristics measured during the pulses, before (blue circles) and after (open squares) the volatile transition (see corresponding symbols in Figure 6b). d) Dependence of E_{th} in Mott insulators and semiconductors. Threshold electric field (inducing avalanche breakdown) as a function of the Mott gap E_G for various AM_4Q_8 compounds. The solid blue curve corresponds to a power law dependence $E_{th} \propto E_G^{2.5}$. Inset: comparison of the threshold fields versus gap dependence for the AM_4Q_8 compounds and for classical semiconductors. The solid blue line displays the universal law E_{th}[kV/cm] = 173 (E_G[eV])$^{2.5}$ observed for semiconductors. Reproduced with permission.[102] Copyright 2013, Macmillan Publishers Limited.

behavior provides a strong evidence that supports the avalanche breakdown scenario in these Mott insulators.

4.2. Modeling of Avalanche Phenomena in Mott Insulators

Avalanche breakdown in semiconductors[105–107] is the consequence of an impact ionization process: some electrons accelerated by an electric field can promote by direct impact other electrons from the valence band to the conduction band, hence creating electron-hole pairs.

In the same way, avalanche breakdown in Mott insulators could result in the massive creation of doublons (i.e., doubly occupied sites) and holes at the local scale, and hence break locally the Mott insulating (MI) state into a correlated metallic (CM) state. The volatile resistive switching was therefore modeled by implementing a resistor network made of an array of cells (**Figure 7**b) which represents a small portion of the crystal that may be of a few nanometers.[102,108] Each cell is either in MI or in CM state, and its resistance is either in high or low resistance state, respectively R_{MI} or R_{CM}. The transition between both states was modeled using the energy landscape presented in Figure 7a. The CM state has a higher energy E_{CM} than the MI state, since the compounds are generally in the Mott insulating state and the correlated metal state is metastable. The application of an electric field increases the energy level of the MI state, and thus lowers the difference in energy between both states. In this model the MI → CM transition is mainly dependant on the electric field:

$$P_{MI\rightarrow CM} = \nu e^{-\frac{E_B - q|\Delta V|}{kT}} \quad (1)$$

(ν is an attempt rate, q is the charge, T is the temperature and ΔV is the local voltage drop for the considered cell) while the CM → MI transition is a thermally activated relaxation from a metastable state:

$$P_{CM\rightarrow MI} = \nu e^{-\frac{E_B - E_M}{kT}} \quad (2)$$

This model reproduces the experimental phenomenology of the RS (i.e., time evolution of current and voltage and $I(V)$ characteristic) and provides a microscopic view of the transition.[102,108,109] Under an applied electric field, insulating sites transform into metallic at a rate given by Equation (1). If the transformation rate overcomes the relaxation one of Equation (2), then metallic sites accumulate with time (regime depicted in yellow in Figure 7d) in the material. This process continues until a critical density of CM regions sets off an avalanche-like process, which ends in the formation of a conductive path connecting the electrodes (regime in green in Figure 7d). A typical filament is presented in Figure 7e, just after its creation which leads to a resistive switching. After percolation, the number of metallic sites still goes on increasing (regime represented in pink in Figure 7d), although at a lower rate, as long as the electric field is applied. In these three different regimes, the rate of accumulation of metallic sites accelerates when the applied electric field increases. As a consequence for higher voltage the slope for the creation of metallic sites is steeper (yellow region in Figure 7d) and the time for the creation of the filament is shorter (green region in Figure 7d). It explains the decrease of delay time after which the transition occurs vs the applied voltage as found

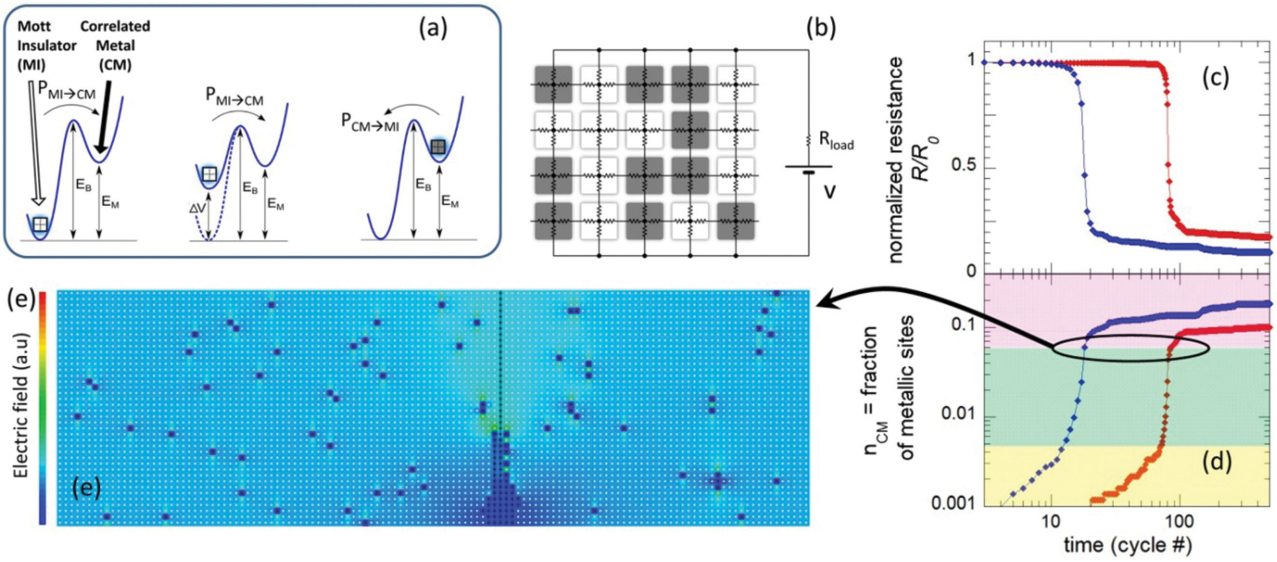

Figure 7. a) Energy landscape model used to simulate the Mott IMT driven by an external electric field. b) This landscape is applied to every cell of the resistor network, where grey and white dots represent respectively cells in the MI and CM (transited) states. c) Resulting simulated evolution of normalized resistance R/R_0. The applied voltage is higher for the blue curve than for the red one. b) Associated increasing fraction of metallic sites in the resistor network. The yellow, green, and pink areas correspond respectively to the increase of metallic cells before, during and after the creation of the filamentary percolating path. e) Representation of the resistor network and associated electric field, just after the creation of this filament. Reproduced with permission.[113] Copyright 2014, Wiley-VCH Verlag GmbH & Co.

experimentally (see Figure 6a).[108,109] Finally, calculations combining the energy landscape model with a thermal model confirm that the onset of the resistive transition is solely driven by a purely electronic transition, while Joule heating occurs once the metallic filament is created and the current starts to raise in the circuit.[109]

4.3. Avalanche Phenomena in Mott Insulators: A Universal Property

The avalanche breakdown phenomenon is a universal property of classical semiconductors. According to the modeling detailed above, avalanche phenomenon should also occur in any Mott insulator provided that the electric field is strong enough to destabilize sufficiently the Mott Insulating state. Recent experiments support that the avalanche breakdown as observed in the AM_4Q_8 compounds can be found in other narrow gap Mott insulators. Avalanche breakdown was indeed demonstrated in the famous Mott Insulators $(V_{1-x}Cr_x)_2O_3$ and $NiS_{2-x}Se_x$.[108] **Figure 8** shows that these compounds exhibit a similar behavior as $GaTa_4Se_8$ with a sharp transition onset at a threshold electric field of the order of a few kV/cm. In the same way, the avalanche breakdown model might also explain the resistive switchings in Mott insulators like Sr_2CuO_3 and $SrCuO_2$,[90] or κ-$(BEDT\text{-}TTF)_2Cu[N(CN)_2]Br$[93] as the threshold fields and $I(V)$ characteristics observed for these compounds are quite similar. Avalanche breakdown appears therefore as a universal property of narrow gap Mott insulators. This transition can be considered as a new type of Mott transition. However avalanche breakdown differs from the filling-control or bandwidth-control IMT described in Section 2. These classical Mott transitions are indeed static bulk properties while avalanche breakdown appears as a dynamical and filamentary Mott transition. This electric field controlled IMT will be noted thereafter as type 5.

5. Non-Volatile Resistive Switching in Mott Insulators

5.1. Evidence of Electric Field Driven Non-Volatile Mott IMT

For electric fields well above the avalanche threshold field involved in the volatile transition, the AM_4Q_8 compounds exhibit a non-volatile resistive switching.[13] Indeed, the application on AM_4Q_8 crystals of short voltage pulses of large amplitude induces a non-volatile drop of their resistance, namely the low bias resistance measured after the end of the pulse remains at a low resistance value. **Figure 9**a shows the resistance vs temperature curve of a GaV_4S_8 crystal measured at low bias level in the pristine and transited states. Whereas the pristine curve is typical of an insulator, the transited state is characteristic of a metallic-like material, showing a drop a resistance of several orders of magnitude. As observed for the volatile transition, the non-volatile transition appears in all AM_4Q_8 compounds (see the examples of GaV_4S_8, $GaMo_4S_8$ and $GaTa_4Se_8$ shown in Figure 9).[13,110,111] Interestingly, Figure 9c,d demonstrates that this non-volatile resistive switching behavior can also be extended to the other Mott insulators such as $V_{1.7}Cr_{0.3}O_3$ and NiS_2, where the volatile transition has been previously displayed. These recent results suggest that both the volatile and non-volatile resistive switchings could be generalized to the entire class of narrow gap Mott insulators.

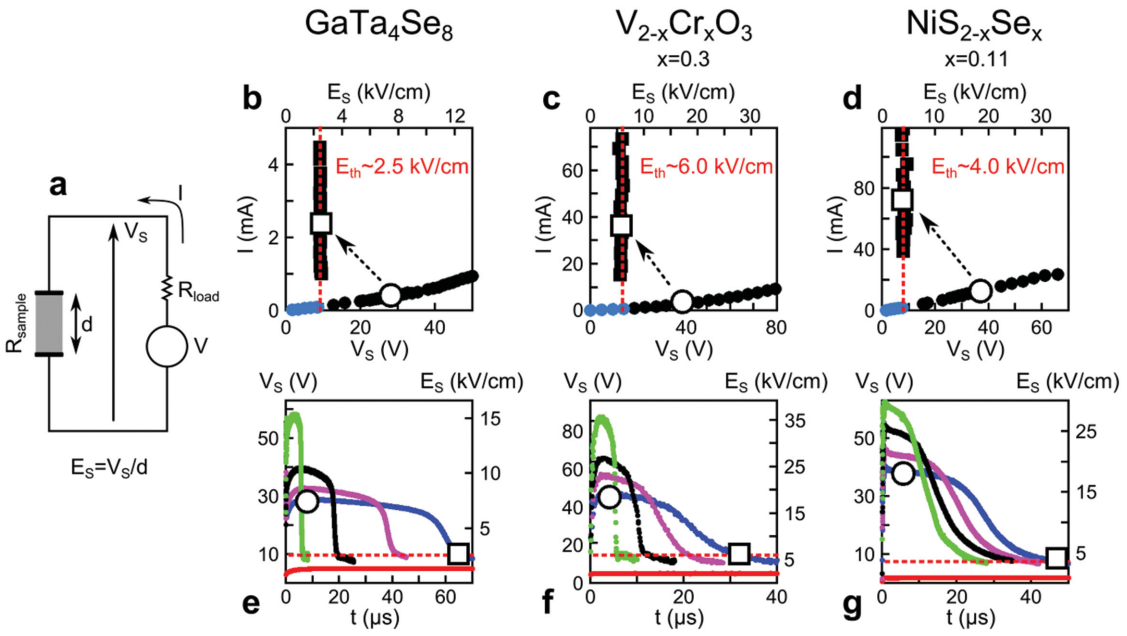

Figure 8. a) Schematics of the experimental setup. b–d) Universal dielectric breakdown *I*–*V* characteristics and e–g) time dependence of the sample voltage $V_S(t)$ are displayed for three different types of narrow gap Mott insulators. Blue dots correspond to the region below E_{th}, where no breakdown is observed. Black symbols correspond to the *I*–*V* characteristic in the resistive switching region, above E_{th}. The black dots show the initial *I*–*V*, before the breakdown, and the black squares indicate the final state. The open symbols highlight a particular breakdown transition for easier visualization. Measurements on $GaTa_4Se_8$ were performed at 77 K,[8] on $V_{2-x}Cr_xO_3$ ($x = 0.3$) at 164 K and on $NiS_{2-x}Se_x$ ($x = 0.11$) at 4 K. Reproduced with permission.[108] Copyright 2013, Wiley-VCH Verlag GmbH & Co.

Moreover the detailed study of this non-volatile transition has shown that the successive application of unipolar electric pulses to these Mott insulators makes the resistance switch back and forth between high and low resistance states.[13] This reversibility of the non-volatile transition enables envisioning memories based on these materials.[112] Noteworthy intermediate levels between high and low resistance states can be reached,[99] which could be of interest for multi-level data storage or memristive applications.

5.2. From Volatile to Non-Volatile Resistive Switching: Control of SET and RESET

The existence of a volatile resistive switching (RS) above a threshold electric field which becomes non-volatile at higher field is a specific fingerprint of narrow gap Mott insulators. Recent experiments provide insight into the relationship between these two types of switchings.[113] **Figure 10**a,b show, for example, that a series of seven identical pulses yields a non-volatile transition while each of these pulses applied independently would only trigger a volatile resistive switching. Such an evolution from single pulse/volatile RS to multipulse/non-volatile RS can be rationalized on the basis of the model of resistor network with two competing phases already introduced in Section 4.2. This model described on Figure 7 indeed predicts that the application of an electric field in a Mott insulator induces an accumulation of metallic sites. A volatile resistive switching is triggered above a critical accumulation threshold, through the creation of a conductive percolating path. This model also predicts, as shown in the upper part of Figure 7d, that the number of metallic sites still goes on increasing after the creation of the filament, as long as the electric field is applied. Simulations show that this accumulation effect corresponds to an increase of the filament diameter. In the experiments described above, the filament diameter is then much larger after application of a series of a few consecutive pulses than after a single pulse. These simulations thus strongly suggest that the observed non-volatile stabilization of the RS ("SET transition") is directly related to the growth of the conducting filament. This concept of critical size above which the filament becomes stable is consistent with classical mechanisms of nucleation and growth processes, where stabilization of a phase becomes possible only above a critical size.[114]

Another appealing prediction of the model of resistor network with competing phases is that the relaxation of metallic domains toward their more stable (Mott) insulating state is thermally activated. This suggests that Joule self-heating could be used to promote the RESET transition to the high resistance state.[113] Figure 10c shows that the application of a very long pulse with electric field chosen to optimize the competition between relaxation (heating effect) and creation (electric field effect) of metallic sites, is indeed efficient to induce the RESET. This long pulse relaxes the resistance to a value very close to the pristine state, which may indicate the quasi-complete dissolution of the filament. On the other hand, no RESET transition is observed when the duration of the pulse is reduced by a factor 4 (see Figure 10c) which fully supports a thermal mechanism for the dissolution of the filament. Schemes of the filament evolution suggested by these experiments are shown in Figure 10.

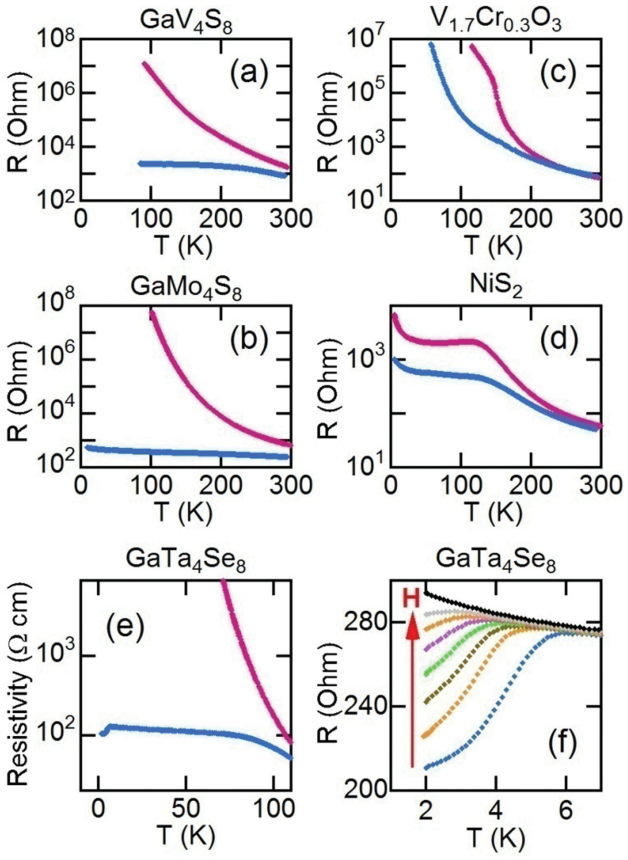

Figure 9. Variation of resistance as a function of temperature for various narrow gap Mott insulators in pristine state (pink curves) and after the application of an electric pulse inducing a non-volatile resistive switch (blue curves), in a) GaV_4S_8, b) $GaMo_4S_8$, c) $V_{1.7}Cr_{0.3}O_3$, d) NiS_2, and e) $GaTa_4Se_8$. f) resistance versus temperature for various magnetic fields (from 0 to 5 Tesla) in a transited $GaTa_4Se_8$ single crystal.[99]

To sum up, these experiments demonstrate the relevance of the model of resistor network with two competing phases in the description of both the volatile and non-volatile resistive switchings. According to this model, the volatile resistive switching corresponds to the creation of a conducting filament too thin to be stabilized after the end of the electric field pulse. Conversely, for a non-volatile resistive switching, the thickness of filament is sufficiently large to allow its stabilization after the pulse. **Figure 11** summarizes this scenario and provides schematic representations of the evolution of the filament during the volatile, the "SET" and "RESET" transitions. Finally, a very clear strategy of electric pulses application emerges from this work: applying short multipulses with large electric field for the SET and long single pulses with low electric field to promote the RESET.

5.3. Electric-Field-Induced Electronic Phase Separation and Resistive Switching

The model of resistor network with competing phases successfully describes key features of a macroscopic property, the

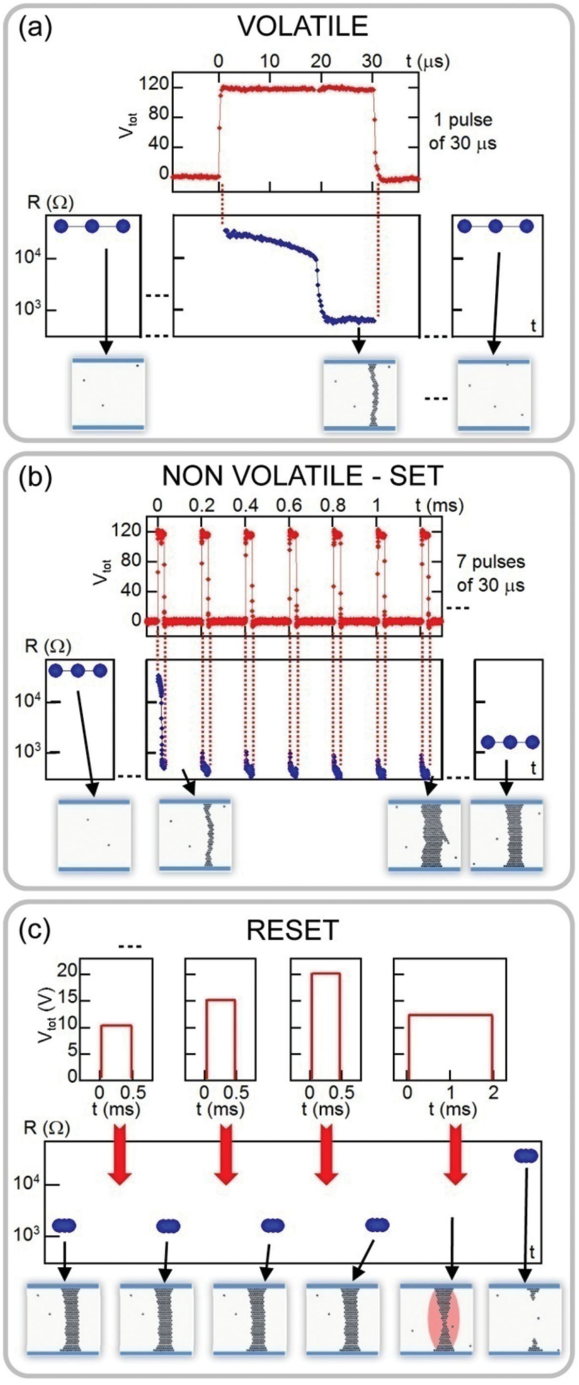

Figure 10. Resistance variation of a GaV_4S_8 crystal, before, during and after applying a) 1 pulse of 30 μs/120 V, and b) a train of 7 pulses of 30 μs/120 V every 200 μs leading to SET non-volatile transition. As expected, the resistance drop during the first pulse shown in (b) is similar to the one occurring during the single pulse in (a). Noteworthy the resistance does not go back to a high resistance state between and during the subsequent pulses. The resistances before and after the application of the (series of) pulses are measured at low bias and are displayed as blue circles. c) Pulse duration impact on the RESET transition in a GaV_4S_8 crystal. 500 μs pulses in the 10–20 V range do not affect resistance level, whereas a 2 ms /12 V pulse induces the RESET transition. The additional sketches illustrate the evolution of the conductive filament through the application of successive pulses.

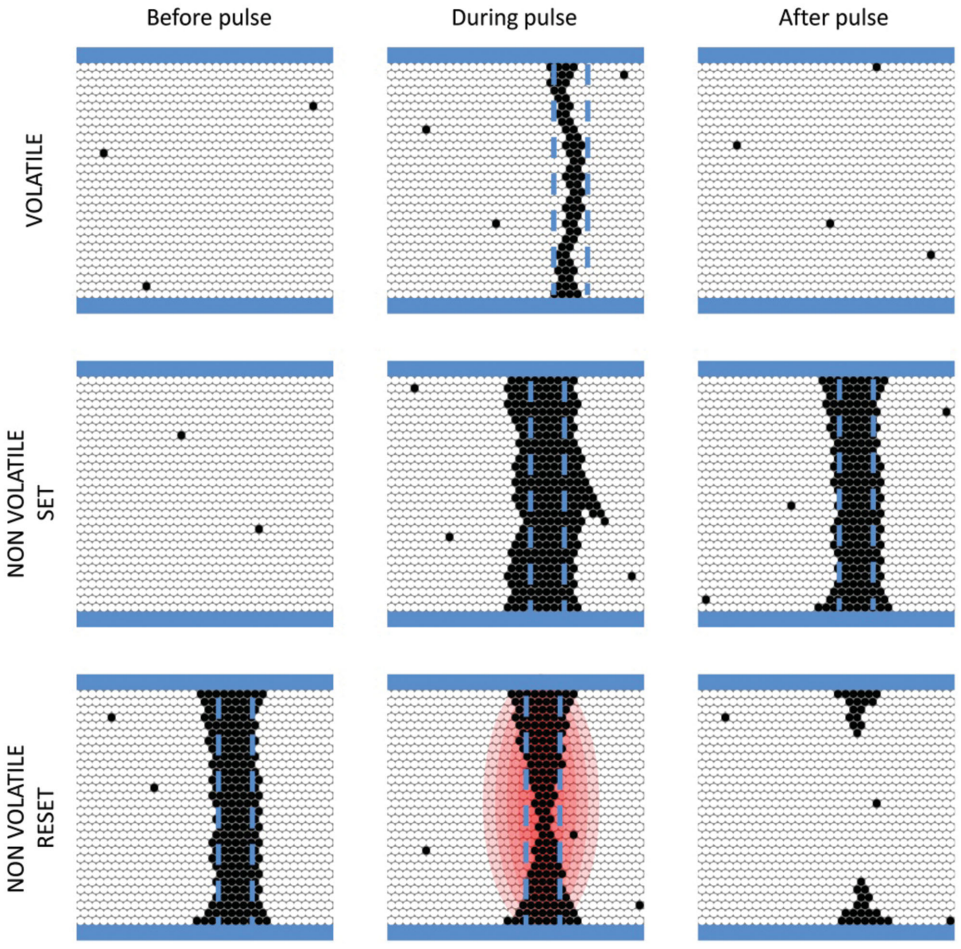

Figure 11. Schematic illustration of the filament evolution before, during and after the application of a pulse inducing a volatile transition, a "SET" non-volatile transition and a "RESET" non-volatile transition. White and black domains represent respectively Mott Insulating and correlated metal regions of the material. Top and bottom electrodes are depicted in blue, and dashed blue lines represent a critical radius of stability for the filament.

volatile resistive switching. It also suggests that new conducting domains should appear at a microscopic level after a non-volatile RS. Scanning tunnel microscopy/spectroscopy (STM/STS) experiments have been carried out on freshly cleaved $GaTa_4Se_8$ single crystals before and after a non-volatile resistive switching to explore this hypothesis.[12,98,115] These experiments have revealed that the non-volatile RS is related to an electronic phase separation at the nanoscale. While the surface topography of pristine crystals is structureless, filamentary structures made of nanoscale heterogeneities with a typical size of 30–70 nm appear after RS, qualitatively oriented along the direction of the electric pulses (**Figure 12**a,b).[12] The analysis of STS map shown in Figure 12d reveals that, beside an insulating matrix with STS spectra similar to the pristine state (green areas, curves A in Figure 12e-f), these RS-induced nanoscale heterogeneities consist in two different kinds of domains. The first ones are metallic (red areas, curve B in Figure 12d–f) and the others super-insulating (blue-violet areas, curve C), that is, with a low bias conductance smaller than the pristine one. Moreover the analysis of the tunnel conductance vs voltage measured on each point of Figure 12d was used to extract the distribution of the local electronic gaps. Before resistive switching, the distribution of the gap values is homogeneous around 200 meV in the pristine state, as shown in Figure 12g. Conversely, Figure 12h shows that new gapless regions appear after RS (the metallic regions in red on Figure 12d), whereas the super-insulating regions (blue-violet regions in Figure 12d) correspond to a continuum of larger gaps between 200 and 700 meV, embedded in an undisturbed matrix whose gap distribution is centered around 200 meV.[115]

The STM experiments demonstrate therefore that for the nonvolatile resistive switching the metallic filamentary paths are made of a percolating granular metallic phase instead of a percolating metallic phase as suggested by the modeling work. This is further confirmed by transport measurements performed after a non-volatile resistive switching. The resistance of the crystal is then well described by a two resistance model considering a granular metallic phase (with power law temperature dependence) placed in parallel with an insulating pristine-like phase (with an activated law temperature dependence).[99]

The nanodomains revealed by STM were carefully investigated by energy dispersive X-ray spectroscopy, and by transmission electron microscopy.[110] No chemical composition change nor any crystallographic symmetry breaking or amorphisation between the electrodes were detected at the nanometric scale.

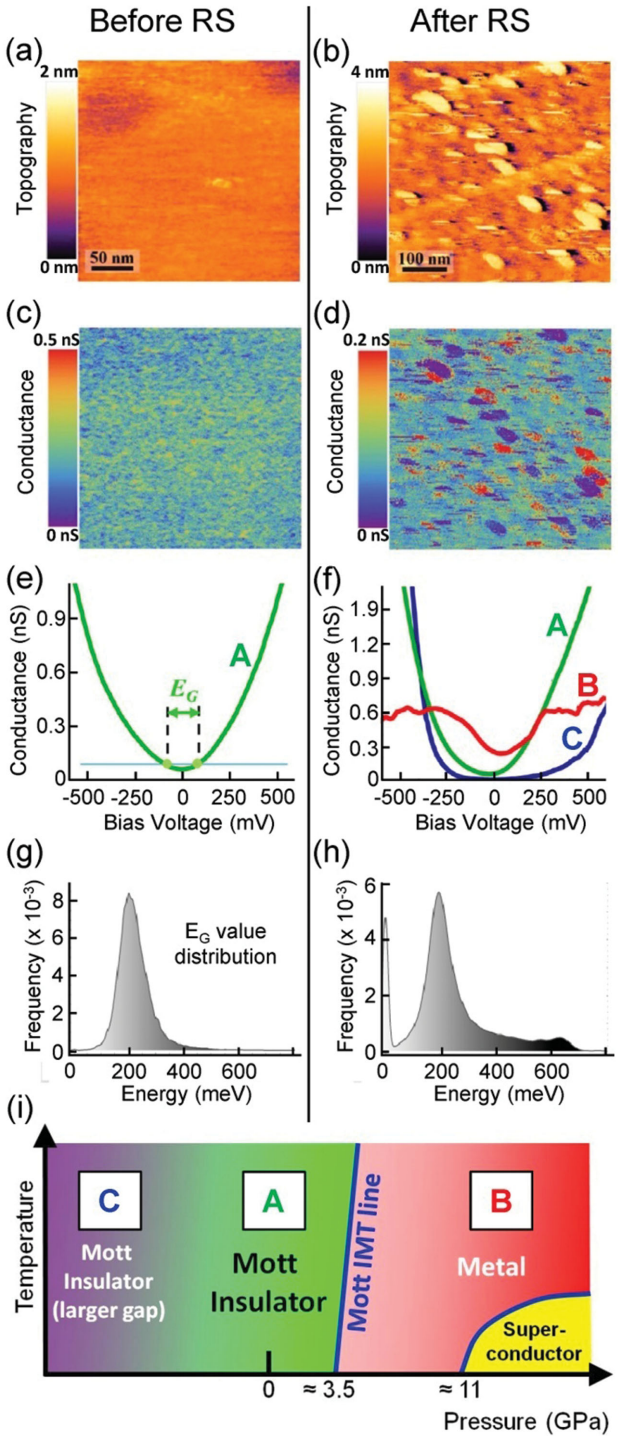

Figure 12. STM/STS study of a freshly cleaved $GaTa_4Se_8$ surface, before and after RS: small-scale topographic STM images of a) the pristine crystal and b) the transited crystal. c) Conductance map measured at –200 mV of the area shown in (a) showing a homogeneous electronic state. d) Conductance map measured at –200 mV of the area shown in (b) exhibiting strong electronic heterogeneities. e) Representative tunneling conductance spectrum of a pristine cleaved crystal. The gap $E_G \approx 100$–200 meV measured by optical and resistivity measurements is indicated by the threshold blue line. f) Tunneling spectra corresponding to zones A (green), B (blue–violet), and C (red) displayed on image (d). The dI/dV spectra of the zone A (in green) are similar to the one of the insulating pristine samples; the spectra from zone B (blue–violet) are more insulating and hence are called superinsulating while the spectra from zone C (in red) are "metallic-like". g,h) Distribution of the electronic gap extracted from a 500 nm × 500 nm STS map, in the pristine (g) and transited state (h). i) Schematic temperature – pressure phase diagram of the Mott insulator $GaTa_4Se_8$ in its pristine state. For negative pressure (expansion), the Mott-Hubbard gap increases continuously. For positive pressure (compression), a discontinuous first order transition occurs at a critical pressure (≈3.5 GPa), and the compound undergoes a Mott IMT. Above ≈11 GPa, $GaTa_4Se_8$ becomes superconducting with critical temperature in the 4–7 K range.[43] Adapted with permission.[115] Copyright 2013, American Chemical Society.

This excludes the formation of conducting bridge-like filaments,[116] amorphous-crystalline transition as observed in phase change materials[117] or phase transition similar to the monoclinic-tetragonal phase change observed in VO_2 (see discussion in Section 2.3).

Moreover STM/STS studies have revealed the extreme sensitivity of the crystal surface to the electric field generated by the STM tip. Applying voltages above a threshold value between the STM tip and the surface indeed allows switching nanodomains of typical diameter 10–20 nm. These pristine—metal or pristine—superinsulating switchings are reversible and always accompanied by a small topographical change of the surface.[115] For higher tip-surface voltage, the surface deformation is drastically enhanced and leads ultimately to an irreversible indentation of $GaTa_4Se_8$ crystal by the STM tip.[98] Both effects are completely unusual and provide clear evidence of a strong electromechanical coupling in $GaTa_4Se_8$.

5.4. Towards a Microscopic View of the Resistive Switching in Mott Insulators

The STM/STS experiments have unveiled a particularly important feature of the non-volatile resistive switching in AM_4Q_8, that is, the existence of electric field induced metallic nanodomains without any evidence of crystallographic symmetry breaking (CSB) with respect to the pristine Mott insulating phase. Interestingly, this is reminiscent of the coexistence of phases sharing the same crystallographic structure that develops across the Mott IMT line in Cr-substituted V_2O_3.[118] This absence of CSB in transited AM_4Q_8 thus reminds the behavior expected across the "type 1" Bandwidth Controlled Mott transition discussed in Section 2. This suggests that the metallic domains shown in Figure 12d could correspond to compressed domains of $GaTa_4Se_8$ which have crossed the IMT line shown in Figure 12i.

This hypothesis was tested using the superconducting transition observed at low temperature (T_C = 4–7 K) in compressed $GaTa_4Se_8$ above 11 GPa.[43] Figure 9e,f show that the resistance drops below 6K in a transited crystal of $GaTa_4Se_8$. This resistance drop is gradually suppressed by a magnetic field of 5 T, that is, a value in the same range as the critical field H_{c2} determined on bulk $GaTa_4Se_8$ under pressure.[43] Moreover, the resistance drop displayed in Figure 9e,f is only partial and does not go to zero. All these features indicate the presence of granular superconductivity, that is, of disconnected and non-percolating superconducting domains after resistive switching in $GaTa_4Se_8$. The absence of percolation is clearly consistent with the spatial

distribution of metallic (red) domains depicted in Figure 12d, which are disconnected from each other. To sum up, the presence of granular superconductivity directly proves the presence of compressed metallic domains in transited crystal of $GaTa_4Se_8$.

The existence of compressed (metallic) domain has an interesting consequence: from simple arguments of volume conservation within the $GaTa_4Se_8$ crystal volume, one can infer that expanded domains should coexist with the compressed ones. As discussed in previous work[25] and shown in Figure 12i, expanding a Mott insulator leads to increase its Mott-Hubbard gap. This scenario thus rationalizes the STM/STS studies displayed in Figure 12. In particular, the seemingly complex "electronic patchwork" shown in Figure 12d simply consists in a set of compressed metallic and neighboring expanded super-insulating domains, embedded in a pristine insulating matrix, and organized along filamentary pathways.

More generally, all these results suggest that the electronic avalanche breakdown induces the collapse of the Mott insulating state into a correlated metallic state. This effect occurs at the local scale and leads to the formation of a granular conductive filaments formed by compressed metallic domains and expanded "superinsulating" domains. This idea that a purely electronic effect, the avalanche, is responsible for a strong response of the lattice is quite natural in the context of Mott IMT physics. For example, the driving force of all Mott IMT is also purely electronic and the lattice response (e.g., the volume contraction at the bandwidth controlled IMT)[30] appears a simple consequence of this electronic effect.[26] The Dynamical Mean Field Theory indeed predicts that this lattice response follows from a dramatic change in the electronic wavefunction across the IMT, which has a direct effect on the compressibility of the lattice.[26] The strong sound velocity anomalies reported at the IMT in Cr-substituted-V_2O_3[119] and in molecular Mott insulators[120,121] provide direct evidence of this effect. The electric-field-induced resistive switching hence appears as a new type of out of equilibrium Mott insulator-to-metal transition and as a universal property of narrow gap Mott insulators. Finally the modeling work of this original mechanism of RS supplies strategies to control both SET and RESET non-volatile transitions. This will be valuable for the realization of efficient ReRAM devices based on narrow gap Mott insulators. The fabrication of such devices and the characterization of their performances are addressed in Section 6.

6. ReRAM Devices Based on Avalanche Breakdown in Narrow Gap Mott Insulators

The resistive switching based on electric field controlled IMT discovered on Mott insulator compounds like AM_4Q_8,[12,13] $V_{1.7}Cr_{0.3}O_3$ or NiS_2 leads to non volatile transitions which makes them potential candidates for ReRAM applications. Studies on this type of ReRAM are scarce and mainly focused on GaV_4S_8. The following sections present therefore the realization of metal insulator metal (MIM) devices using the narrow gap Mott insulator GaV_4S_8 and describe the performances obtained on these devices in the context of ReRAM applications.

6.1. Preparation of GaV_4S_8 Thin Active Layers and GaV_4S_8 Based MIM Structures

The deposition of GaV_4S_8 material in the form of thin layers has been investigated both by non-reactive RF magnetron sputtering in pure argon[122] and by reactive process in Ar/H_2S mixture[123] using a stoichiometric GaV_4S_8 target.[124] A process parameter window enabling to obtain thin films has been determined both in non-reactive[122] and in reactive gas mixtures.[123] For both approaches, GaV_4S_8 thin films need to be annealed in the 450–600 °C range to exhibit a crystalline structure, as checked by XRD analysis (**Figure 13**a). For films deposited in pure Ar, the annealing is performed with excess sulfur, whereas thin films deposited in reactive phase H_2S/Ar do not need any enrichment to achieve the targeted sulfur stoichiometry. After annealing, the stoichiometric polycrystalline layers crystallize with the expected lacunar spinel structure, (Figure 13a), and exhibit a granular morphology as revealed by the SEM image of a 100 nm annealed thick film elaborated with 1% H_2S content (Figure 13b).

Several MIM structures Au/GaV_4S_8/Au were subsequently realized (Figure 13e,f) using these well crystallized GaV_4S_8 thin layers. TEM analyses reveal the excellent crystalline quality of the GaV_4S_8/Au interface at top and bottom electrodes, with GaV_4S_8 atomic planes clearly visible at 2 nm from the interface (Figure 13c), without any interfacial amorphous layer.[125]

6.2. Resistive Switching in GaV_4S_8 MIM Structures

Resistive switching experiments were performed on GaV_4S_8 MIM structures. A non-volatile resistive switching can be induced by applying electric pulses to polycrystalline GaV_4S_8 thin films. The resistance versus temperature dependence of the GaV_4S_8 polycrystalline thin layer, displayed in **Figure 14**b, changes from an insulating state in the pristine state (R_{OFF} = red curve) to a conductive one (R_{ON} = blue curve) after the application of short electric pulses in the 500 ns–10 µs range. This is completely similar to the resistive switching observed previously on single crystal (see comparison in Figure 14a,b). Moreover, a significant difference between R_{ON} and R_{OFF} is still observable on thin films at 300 K (Figure 14b). The pulse protocol described in Section 5.2 was therefore tested at room temperature in order to control the SET and RESET transitions on GaV_4S_8 MIM structures. This voltage pulse protocol alternates a series of seven identical short pulses of large amplitude to generate the SET transition with a single long and low amplitude pulse to generate the RESET transition. Using this pulse protocol a reversible switch back and forth between the high and low resistance states was observed at room temperature on this Au/GaV_4S_8/Au MIM structure (Figure 14).

6.3. Performances of GaV_4S_8 Based ReRAM Devices

Electrical performances such as endurance, scalability, and retention times were evaluated on GaV_4S_8 MIM structures. The endurance was measured on a GaV_4S_8 based device and exceeds 65 000 successive cycles with less than 0.01% error rate.[125]

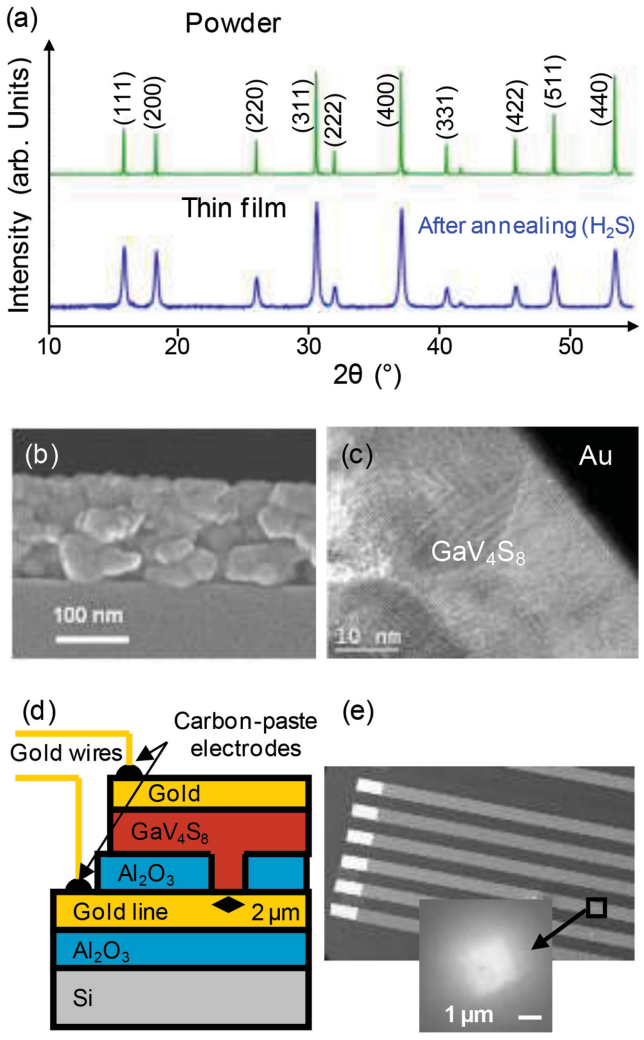

Figure 13. Typical characteristics of GaV_4S_8 thin layers (from top to bottom): a) X-ray diffraction pattern of a 400 nm thick layer after 1 h annealing at 873 K under H2S flow and comparison with the one of home-synthesized powder used as a reference; b) SEM image in cross section of a 100 nm thick GaV_4S_8 layer elaborated with 1% H2S after annealing at 813 K; c) high magnification TEM picture of the bottom GaV_4S_8/Au interface within a 50 µm × 50 µm Au/GaV_4S_8/Au MIM structure; d) Schematic drawing of the 2 µm × 2 µm MIM structure cross-section; e) SEM images of the corresponding substrate before deposition of the GaV_4S_8 layer (surface view).

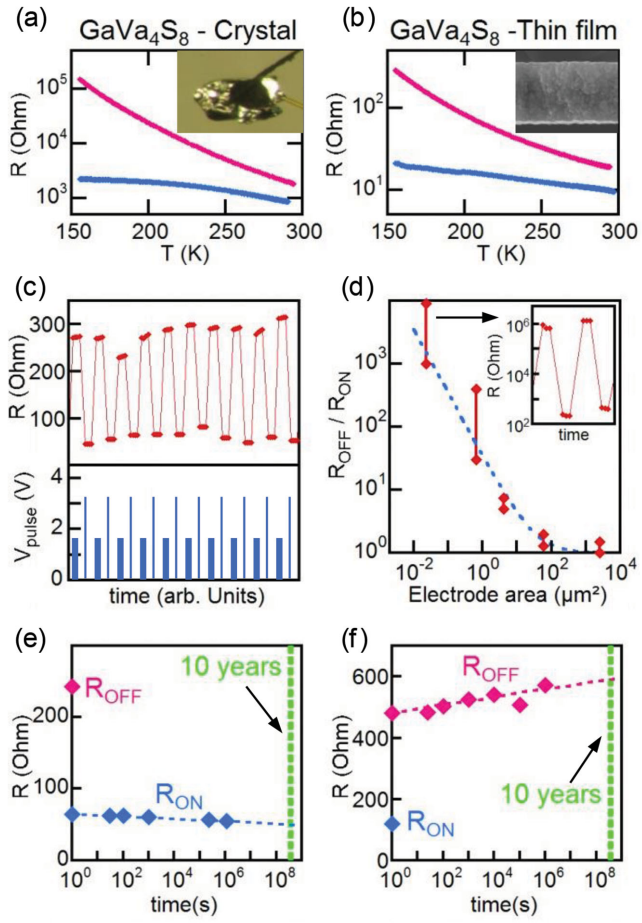

Figure 14. Typical electrical characteristics of GaV_4S_8 MIM devices. Gold is used for the metallic electrodes of the thin-layer-based MIM devices. a,b) Comparison of the temperature dependences of high and low resistive states for a) a 300 µm GaV_4S_8 single crystal and b) a 400 nm thick GaV_4S_8 thin layer obtained in pure Ar phase (50 µm × 50 µm pad size). c) Resistive switching cycles obtained on 2 µm × 2 µm and 150 nm thick GaV_4S_8 based MIM structure in series with R_{load} = 10 Ω, by applying successively a multipulse sequence (seven 3.2 V/500 ns pulses, period 3.5 µs) and single 1.6 V/500 µs pulses. d) Variation of the R_{OFF}/R_{ON} ratio vs the electrode area. The dotted line indicates the dependence expected for a simple model of creation / full dissolution of a single filament per memory cell. Inset: RS cycles obtained with a 150 nm × 150 nm pad size exhibiting R_{OFF}/R_{ON} ratio larger than one thousand. e,f) Evolution of e) R_{ON} and f) R_{OFF} versus time for two different 2 µm × 2 µm MIM structures with retention extrapolation to 10 years, and comparison with their initial R_{OFF} and R_{ON} levels. The performances evaluated in (c–f) were obtained at 300 K.

The downscaling properties were also investigated on MIM structures[125] with electrode pad size ranging from 50 µm × 50 µm down to 150 nm × 150 nm. As displayed in Figure 14 d the R_{OFF}/R_{ON} ratio strongly increases with decreasing pad area and reaches values larger than 1000 for pads of 150 nm × 150 nm. This result can be easily explained considering the filamentary model depicted in Section 5. As long as the cycling involves the creation/full dissolution of a single filament, R_{OFF} is indeed expected to scale with the inverse of the pad area 1/S while R_{ON} is expected to depend only on the resistance of few filamentary conducting paths covering a small area. As a consequence, R_{OFF}/R_{ON} should increase as 1/S for small pads area, which is observed experimentally for areas below 5 µm² (Figure 14d) and should keep increasing as long as pad sizes remain larger than the filamentary conducting paths. R_{OFF}/R_{ON} ratios larger than the 10^3–10^4 current values can thus be expected with further pad size downscaling.

The stability of high and low resistive states obtained on MIM structures has been investigated at room temperature. Extrapolation of R_{OFF} and R_{ON} to 10 years shows respectively slight increase and decrease of these resistance levels (Figure 14e,f). Both states exhibit therefore good retention time which is promising for data storage.

Another interesting feature of the switching mechanism observed in narrow gap insulators is that it enables a simple

way to tune the SET voltage. Indeed the resistive switching is driven by electric field of the order of kV/cm. The SET voltages used on single crystals (typically 30–50 V for 10–30 µm inter-electrode distance) largely decreases on thin films (down to 1.5 V for 150 nm). SET voltage value lower than 1 V is therefore expected for sub-100 nm thick thin films targeted in future devices. Finally writing time (SET transition) of 7 × 15 ns and erasing time (RESET transition) as short as 500 ns were obtained in GaV_4S_8 planar structures.[125]

To summarize, the endurance of Mott-RAM devices is very promising compared to values ranging from 10^3 to 10^7 cycles currently obtained in Flash technology.[112] The writing time of 7 × 15 ns and the erasing time of 500 ns are favorable compared to characteristics achieved in Flash technology, that is, writing time of 1 µs and even much better than the typical erasing times of 10 ms. In addition, the writing/erasing voltage in the 1 V range stands as a huge advantage when compared to the 12 V reported for Flash memories.[112] Among other ReRAM emerging technologies, Mott insulator based ReRAM devices could be thus considered as really promising candidates to take over the Flash technology.

Insulator to Metal Transition	Resistive switching mechanism		Mott insulators	Correlated insulators
Temperature-Controlled IMT (type 2 and 4)	Thermal		• $(V_{0.99}Cr_{0.01})_2O_3$ [60] • $NiS_{1.45}Se_{0.55}$ [61, 62]	• VO_2 [63,64] • NbO_2 [65] • Ca_2RuO_4 [5,66] • V_2O_3 (AFI → metal) [67,68,69] • Fe_3O_4 [70,71]
Filling-Controlled IMT (type 3)	Valence Change	Filamentary	• NiO [10,83,84] • CuO [83,85]	
		Interfacial	• $YBa_2Cu_3O_{7-x}$ [81] • La_2CuO_4 [8]	$Pr_{0.7}Ca_{0.3}MnO_3$ [79]
Electric Field-Controlled IMT (type 5)	Avalanche-breakdown-induced electronic phase separation		• **$NiS_{2-x}Se_x$** [108] • **$(V_{1-x}Cr_x)_2O_3$** [108] • **AM_4Q_8 (A=Ga, Ge; M= V, Nb, Ta, Mo; Q=S, Se, Te** [12, 13, 102] • Sr_2CuO_3 [90] • $SrCuO_2$ [90] • κ-$(BEDT\text{-}TTF)_2X$ [93]	

Figure 15. Classification of resistive switching mechanisms in Mott and Correlated Insulators depending on the type of IMT involved in the resistance change. Compounds names written in normal, italic and bold characters display respectively non-volatile, mainly volatile and both volatile/non-volatile resistive switching.

7. Conclusion

Insulating state may arise in systems with an integer number of unpaired electrons owing to strong electronic correlations. The most prominent examples of these type of systems, known as Mott Insulators, are $(V_{1-x}Cr_x)_2O_3$, $NiS_{2-x}Se_x$ and AM_4Q_8. There are several ways to destabilize the Mott insulating state. The best known ones consist in either applying pressure (bandwidth-controlled IMT, type 1), changing the temperature in the vicinity of the Mott transition line (temperature-controlled IMT, type 2) or doping the system away from half filling (filling-controlled IMT, type 3). Recently another way to destabilize the Mott insulating state was reported consisting in applying strong electric field. Electric field can indeed initiate a dielectric breakdown of the avalanche type in Mott Insulators which can be considered as an electric-field-controlled IMT (type 5). These insulator-to-metal transitions which emerge from the Mott insulating state are called Mott transitions and do not involve a change in the crystal structure symmetry. Alternatively, many insulating correlated materials like VO_2, Ca_2RuO_4 or Fe_3O_4 display temperature-controlled IMT (type 4) associated with diverse phase changes that all involve crystallographic symmetry breakings.

Temperature, filling or electric-field-controlled IMT which appear in Mott or correlated insulators are interesting in the context of Resistive RAM. Indeed, resistive switchings in Mott or correlated insulators can be classified under three types of mechanisms depending on the type of IMT responsible for the change of resistance (see **Figure 15**). A first type of resistive switching can be explained by a Joule heating induced Temperature-Controlled IMT (type 2 and 4). This thermal mechanism of resistive switching is encountered in Mott insulator systems like $(V_{1-x}Cr_x)_2\ O_3$ ($x \approx 0.01$) and $NiS_{2-x}Se_x$ ($x \approx 0.45$) and in many correlated insulators like VO_2, Ca_2RuO_4,or Fe_3O_4.

A second type of resistive switching observed in correlated and Mott Insulators is based on an ionic migration process. In transition metal oxides migration of oxygen under electric field can indeed induce a filling-controlled IMT (type 3) either along filamentary paths or at the oxide-metal electrode interface. This type of resistive switching first described in band insulators like $SrTiO_3$ is called VCM for Valence Change Memory. Filamentary VCM type resistive switching occurs in Mott insulators like NiO while interfacial VCM type resistive switching occurs for various metal- insulator junctions made of correlated materials like $Pr_{0.7}Ca_{0.3}MnO_3$ or $YBa_2Cu_3O_{7-x}$.

Finally, the last type of resistive switching is related to the electric-field-controlled IMT (type 5) or avalanche breakdown recently reported in Mott insulators. This avalanche breakdown induces the collapse of the Mott insulating state at the local scale and leads to the formation of filamentary conducting paths. Depending on the electric field value these filaments can be either volatile or non-volatile (SET transition). Non-volatile filaments may be destroyed by another electric pulse

thanks to Joule heating (RESET transition). This type of resistive switching is universal to narrow gap Mott insulators. It was already demonstrated in several family of Mott insulators like $(V_{1-x}Cr_x)_2O_3$, $NiS_{2-x}Se_x$ and AM_4Q_8. This new mechanism of resistive switching shows promising features such as resistive switching ratio R_{OFF}/R_{ON} exceeding 10^3, cycling endurance reaching more than 65 000 RS cycles, data retention time till 10 years and writing speed below 100 ns. All these results confirm therefore the high potential of this Mott type resistive switching for ReRAM applications.

Acknowledgements

The authors acknowledge CNano Nord-Ouest, Région Pays-de-Loire and CNRS for funding. The French Agence Nationale de la Recherche (ANR) is also deeply acknowledged for financial supports of these studies within the 'NV-CER' (ANR-05-JCJC-0123–01), 'NanoMott' (ANR-09-Blan-0154–01) and 'Mott-RAM' (ANR-2011-EMMA-016–01) funded projects. The Spanish Ministry of Economy also supported work through the Ramon y Cajal (RYC-2012–01031) programs. Deep thanks are due to P. Diener for critical reading of the manuscript and to C. Guillot-Deudon for her ongoing support to this project. All PhD students, post-docs and assistant engineers involved in the early steps of the studies are deeply and warmly acknowledged: C. Vaju, E. Souchier, V. Guiot, V. Dubost, M. Chligui, K. Khazen, J. Martial and S. Salmon-Bourmand.

Received: March 2, 2015
Revised: May 5, 2015
Published online: July 14, 2015

[1] International Technology Roadmap for Semiconductors, Emerging Research Devices (2011) – http://www.itrs.net/ (accessed: March 2015)
[2] Y. Fujisaki, *Jpn. J. Appl. Phys.* **2013**, *52*, 040001.
[3] H.-S. P. Wong, S. Raoux, S. Kim, J. Liang, J. P. Reifenberg, B. Rajendran, M. Asheghi, K. E. Goodson, *Proc. IEEE* **2010**, *98*, 2201.
[4] J.-G. Zhu, *Proc. IEEE* **2008**, *96*, 1786.
[5] F. Pan, S. Gao, C. Chen, C. Song, F. Zeng, *Mater. Sci. Eng. R Rep.* **2014**, *83*, 1.
[6] Yole Développement – i-micronews reports – Emerging non-volatile memory, http://www.i-micronews.com/mems-sensors-report/product/emerging-non-volatile-memory.html (accessed: March 2015).
[7] R. Waser, M. Aono, *Nat. Mater.* **2007**, *6*, 833.
[8] A. Sawa, *Mater. Today* **2008**, *11*, 28.
[9] R. Waser, R. Dittmann, G. Staikov, K. Szot, *Adv. Mater.* **2009**, *21*, 2632.
[10] K. M. Kim, D. S. Jeong, C. S. Hwang, *Nanotechnology* **2011**, *22*, 254002.
[11] D. S. Jeong, R. Thomas, R. S. Katiyar, J. F. Scott, H. Kohlstedt, A. Petraru, C. S. Hwang, *Rep. Prog. Phys.* **2012**, *75*, 076502.
[12] C. Vaju, L. Cario, B. Corraze, E. Janod, V. Dubost, T. Cren, D. Roditchev, D. Braithwaite, O. Chauvet, *Adv. Mater.* **2008**, *20*, 2760.
[13] L. Cario, C. Vaju, B. Corraze, V. Guiot, E. Janod, *Adv. Mater.* **2010**, *22*, 5193.
[14] I. H. Inoue, M. J. Rozenberg, *Adv. Funct. Mater.* **2008**, *18*, 2289.
[15] The site is the entity on which the unpaired electron can be localized. It usually corresponds to a transition metal ion as, for example, in the numerous transition-metal oxides Mott insulators. However the site can also consist in a cluster of atoms, as in AM_4Q_8 chalcogenides compounds, or even in extended molecule as in κ-(BEDT-TTF)$_2$X.
[16] N. F. Mott, *Proc. Phys. Soc. Sect. A* **1949**, *62*, 416.
[17] J. Hubbard, *Proc. R. Soc. Lond. Ser. Math. Phys. Sci.* **1964**, *277*, 237.
[18] J. Zaanen, G. A. Sawatzky, J. W. Allen, *Phys. Rev. Lett.* **1985**, *55*, 418.
[19] A. Georges, G. Kotliar, W. Krauth, M. J. Rozenberg, *Rev. Mod. Phys.* **1996**, *68*, 13.
[20] G. Kotliar, S. Y. Savrasov, K. Haule, V. S. Oudovenko, O. Parcollet, C. A. Marianetti, *Rev. Mod. Phys.* **2006**, *78*, 865.
[21] G. Kotliar, D. Vollhardt, *Phys. Today* **2004**, *57*, 53.
[22] R. Bulla, T. A. Costi, D. Vollhardt, *Phys. Rev. B* **2001**, *64*, 045103.
[23] The phase diagrams shown in Figure 1 correspond to the solution of the single band Hubbard Hamiltonian, one of the simplest models of correlated electrons, by the dynamical mean-field theory (DMFT). The Hubbard model takes into account only the valence electrons moving between lattice sites, with a hopping term t proportional to the bandwidth W. Electrons interact between each other only when they are located on the same site, through the local Coulomb repulsion U. The DMFT solution becomes exact as the number of neighboring sites increases, and is well suited for two- and three-dimensional experimental systems. More details can be found in other studies.[19,20,21,22]
[24] M. Imada, A. Fujimori, Y. Tokura, *Rev. Mod. Phys.* **1998**, *70*, 1039.
[25] Applying a positive external pressure on a Mott insulator induces a volume contraction which enhances the bandwidth W and thus reduces the Mott-Hubbard gap $E_G \approx U - W$. Conversely a volume expansion leads to an enhancement of the gap E_G.
[26] S. R. Hassan, A. Georges, H. R. Krishnamurthy, *Phys. Rev. Lett.* **2005**, *94*, 036402.
[27] A key issue, discussed in in previous work,[26] is that electronic degrees of freedom are the (only) driving force of the "type 1" Mott – Bandwidth Controlled IMT. The lattice contraction observed at the type 1 IMT in real systems is therefore only a consequence of the softening of electronic degrees of freedom, through the usual electron–phonon coupling.
[28] H. Kuwamoto, J. M. Honig, J. Appel, *Phys. Rev. B* **1980**, *22*, 2626.
[29] A temperature increase corresponds to a vertical path in the phase diagram T/W versus U/W shown in Figure 1a. Indeed, thermal expansion effects in solids usually do not modify significantly neither the bandwidth W nor the repulsion U, thus keeping the U/W ratio constant. Starting from the "PMI" state, there is thus no transition line that can be crossed by increasing temperature.
[30] D. B. McWhan, J. P. Remeika, T. M. Rice, W. F. Brinkman, J. P. Maita, A. Menth, *Phys. Rev. Lett.* **1971**, *27*, 941
[31] P. Limelette, A. Georges, D. Jérome, P. Wzietek, P. Metcalf, J. M. Honig, *Science* **2003**, *302*, 89.
[32] D. B. McWhan, T. M. Rice, J. P. Remeika, *Phys. Rev. Lett.* **1969**, *23*, 1384.
[33] A. Jayaraman, D. B. McWhan, J. P. Remeika, P. D. Dernier, *Phys. Rev. B* **1970**, *2*, 3751.
[34] F. Rodolakis, B. Mansart, E. Papalazarou, S. Gorovikov, P. Vilmercati, L. Petaccia, A. Goldoni, J. P. Rueff, S. Lupi, P. Metcalf, M. Marsi, *Phys. Rev. Lett.* **2009**, *102*, 066805.
[35] D. B. McWhan, J. P. Remeika, *Phys. Rev. B* **1970**, *2*, 3734.
[36] P. Limelette, P. Wzietek, S. Florens, A. Georges, T. A. Costi, C. Pasquier, D. Jérome, C. Mézière, P. Batail, *Phys. Rev. Lett.* **2003**, *91*, 016401.
[37] J. M. Honig, J. Spałek, *Curr. Opin. Solid State Mater. Sci.* **2001**, *5*, 269.
[38] H. Benyaich, J. Jegaden, M. Potel, M. Sergent, A. Rastogi, R. Tournier, *J. Common Met.* **1984**, *102*, 9.
[39] R. Pocha, D. Johrendt, R. Pöttgen, *Chem. Mater.* **2000**, *12*, 2882.
[40] V. Guiot, E. Janod, B. Corraze, L. Cario, *Chem. Mater.* **2011**, *23*, 2611

[41] R. Pocha, D. Johrendt, B. Ni, M. M. Abd-Elmeguid, *J. Am. Chem. Soc.* **2005**, *127*, 8732.
[42] H. Müller, W. Kockelmann, D. Johrendt, *Chem. Mater.* **2006**, *18*, 2174.
[43] M. M. Abd-Elmeguid, B. Ni, D. I. Khomskii, R. Pocha, D. Johrendt, X. Wang, K. Syassen, *Phys. Rev. Lett.* **2004**, *93*, 126403.
[44] R. Pocha, D. Johrendt, B. Ni, M. M. Abd-Elmeguid, *J. Am. Chem. Soc.* **2005**, *127*, 8732.
[45] A. Camjayi, C. Acha, R. Weht, M. G. Rodríguez, B. Corraze, E. Janod, L. Cario, M. J. Rozenberg, *Phys. Rev. Lett.* **2014**, *113*, 086404.
[46] Interestingly, Figure 3b shows that $GaTa_4Se_8$ at 5 GPa (i.e., in the metallic phase close to the Mott IMT line) remains metallic down to the lowest temperature. Conversely, pure V_2O_3 displays, in the same region of its phase diagram, a type 4 temperature-controlled metal-insulator transition at ≈ 165 K (see Figure 2d). This difference between $GaTa_4Se_8$ and V_2O_3 demonstrates the non-universal character of the type 4 IMT occurring in pure V_2O_3.
[47] V. Ta Phuoc, C. Vaju, B. Corraze, R. Sopracase, A. Perucchi, C. Marini, P. Postorino, M. Chligui, S. Lupi, E. Janod, L. Cario, *Phys. Rev. Lett.* **2013**, *110*, 037401.
[48] a) E. Dorolti, L. Cario, B. Corraze, E. Janod, C. Vaju, H.-J. Koo, E. Kan, M.-H. Whangbo, *J. Am. Chem. Soc.* **2010**, *132*, 5704; b) C. Vaju, J. Martial, E. Janod, B. Corraze, V. Fernandez, L. Cario, *Chem. Mater.* **2008**, *20*, 2382; c) B. Corraze, E. Janod, E. Dorolti, V. Guiot, C. Vaju, H.-J. Koo, E. Kan, M.-H. Whangbo, L. Cario, in *Frontiers in Electronic Materials: A Collection of Extended Abstracts of the Nature Conference Frontiers in Electronic Materials*, (Ed.: J. Heber, D. Schlom), Wiley, New York **2012**, p. 116.
[49] T. F. Qi, O. B. Korneta, S. Parkin, L. E. De Long, P. Schlottmann, G. Cao, *Phys. Rev. Lett.* **2010**, *105*, 177203.
[50] C. Weber, D. D. O'Regan, N. D. M. Hine, M. C. Payne, G. Kotliar, P. B. Littlewood, *Phys. Rev. Lett.* **2012**, *108*, 256402.
[51] V. Eyert, *EPL Europhys. Lett.* **2002**, *58*, 851.
[52] J. B. Torrance, P. Lacorre, A. I. Nazzal, E. J. Ansaldo, C. Niedermayer, *Phys. Rev. B* **1992**, *45*, 8209.
[53] H. Park, A. J. Millis, C. A. Marianetti, *Phys. Rev. Lett.* **2012**, *109*, 156402.
[54] W.-P. Hsieh, M. Trigo, D. A. Reis, G. A. Artioli, L. Malavasi, W. L. Mao, *Appl. Phys. Lett.* **2014**, *104*, 021917.
[55] H. Wen, L. Guo, E. Barnes, J. H. Lee, D. A. Walko, R. D. Schaller, J. A. Moyer, R. Misra, Y. Li, E. M. Dufresne, D. G. Schlom, V. Gopalan, J. W. Freeland, *Phys. Rev. B* **2013**, *88*, 165424.
[56] M. Dressel, N. Drichko, *Chem. Rev.* **2004**, *104*, 5689.
[57] J. P. Attfield, *Solid State Sci.* **2006**, *8*, 861.
[58] E. J. W. Verwey. *Nature* **1939**, *144*, 327.
[59] J. Li, C. Aron, G. Kotliar, J. E. Han, *Phys. Rev. Lett.* **2015**, *114*, 226403.
[60] F. A. Chudnovskii, A. L. Pergament, G. B. Stefanovich, P. A. Metcalf, J. M. Honig, *J. Appl. Phys.* **1998**, *84*, 2643.
[61] F. A. Chudnovskii, A. L. Pergament, P. Somasundaram, J. M. Honig, *Phys. Status Solidi A* **1999**, *172*, 131.
[62] F. A. Chudnovskii, A. L. Pergament, G. B. Stefanovich, P. Somasundaram, J. M. Honig, *Phys. Status Solidi A* **1997**, *161*, 577.
[63] J. Kim, C. Ko, A. Frenzel, S. Ramanathan, J. E. Hoffman, *Appl. Phys. Lett.* **2010**, *96*, 213106.
[64] A. Zimmers, L. Aigouy, M. Mortier, A. Sharoni, S. Wang, K. G. West, J. G. Ramirez, I. K. Schuller, *Phys. Rev. Lett.* **2013**, *110*, 056601.
[65] S. Kim, J. Park, J. Woo, C. Cho, W. Lee, J. Shin, G. Choi, S. Park, D. Lee, B. H. Lee, H. Hwang, *Microelectron. Eng.* **2013**, *107*, 33.
[66] F. Nakamura, M. Sakaki, Y. Yamanaka, S. Tamaru, T. Suzuki, Y. Maeno, *Sci. Rep.* **2013**, *3*.
[67] F. A. Chudnovskii, A. L. Pergament, G. B. Stefanovich, P. A. Metcalf, J. M. Honig, *J. Appl. Phys.* **1998**, *84*, 2643.
[68] J. S. Brockman, L. Gao, B. Hughes, C. T. Rettner, M. G. Samant, K. P. Roche, S. S. P. Parkin, *Nat. Nanotechnol.* **2014**, *9*, 453.
[69] S. Guénon, S. Scharinger, S. Wang, J. G. Ramírez, D. Koelle, R. Kleiner, I. K. Schuller, *EPL Europhys. Lett.* **2013**, *101*, 57003.
[70] T. Burch, P. P. Craig, C. Hedrick, T. A. Kitchens, J. I. Budnick, J. A. Cannon, M. Lipsicas, D. Mattis, *Phys. Rev. Lett.* **1969**, *23*, 1444.
[71] A. A. Fursina, R. G. S. Sofin, I. V. Shvets, D. Natelson, *Phys. Rev. B* **2009**, *79*.
[72] M. D. Pickett, R. StanleyWilliams, *Nanotechnology* **2012**, *23*, 215202.
[73] M.-J. Lee, Y. Park, D.-S. Suh, E.-H. Lee, S. Seo, D.-C. Kim, R. Jung, B.-S. Kang, S.-E. Ahn, C. B. Lee, D. H. Seo, Y.-K. Cha, I.-K. Yoo, J.-S. Kim, B. H. Park, *Adv. Mater.* **2007**, *19*, 3919.
[74] T. Driscoll, H.-T. Kim, B.-G. Chae, M. Di Ventra, D. N. Basov, *Appl. Phys. Lett.* **2009**, *95*, 043503.
[75] S.-H. Bae, S. Lee, H. Koo, L. Lin, B. H. Jo, C. Park, Z. L. Wang, *Adv. Mater.* **2013**, *25*, 5098.
[76] A bipolar resistive switching depends on the polarity of the applied pulse: some filament or interfacial states are created with one polarity and destroyed by the opposite one. Conversely, both polarities have similar effects for a unipolar resistive switching.
[77] D. B. Strukov, G. S. Snider, D. R. Stewart, R. S. Williams, *Nature* **2008**, *453*, 80.
[78] T. Fujii, M. Kawasaki, A. Sawa, Y. Kawazoe, H. Akoh, Y. Tokura, *Phys. Rev. B* **2007**, *75*.
[79] a) S. Q. Liu, N. J. Wu, A. Ignatiev, *Appl. Phys. Lett.* **2000**, *76*, 2749; b) A. Sawa, T. Fujii, M. Kawasaki, Y. Tokura, *Appl. Phys. Lett.* **2004**, *85*, 4073.
[80] H. S. Lee, S. G. Choi, H.-H. Park, M. J. Rozenberg, *Sci. Rep.* **2013**, *3*.
[81] a) M. J. Rozenberg, M. J. Sánchez, R. Weht, C. Acha, F. Gomez-Marlasca, P. Levy, *Phys. Rev. B* **2010**, *81*, 115101; b) C. Acha, M. J. Rozenberg, *J. Phys.: Condensed Matter* **2009**, *21*, 045702.
[82] The term "Mott insulator" is used here in its broad sense, including both Mott-Hubbard and charge-transfer insulators.[18]
[83] D. C. Kim, S. Seo, S. E. Ahn, D.-S. Suh, M. J. Lee, B.-H. Park, I. K. Yoo, I. G. Baek, H.-J. Kim, E. K. Yim, J. E. Lee, S. O. Park, H. S. Kim, U.-I. Chung, J. T. Moon, B. I. Ryu, *Appl. Phys. Lett.* **2006**, *88*, 202102.
[84] K. Kinoshtia, T. Okutani, H. Tanaka, T. Hinoki, K. Yazawa, K. Ohmi, S. Kishida, *Appl. Phys. Lett.* **2010**, *96*, 143505.
[85] Takeshi Yajima, Kohei Fujiwara, Aiko Nakao, Tomohiro Kobayashi, Toshiyuki Tanaka, Kei Sunouchi, Yoshiaki Suzuki, Mai Takeda, Kentaro Kojima, Yoshinobu Nakamura, Kouji Taniguchi, Hidenori Takagi, *Jpn. J. Appl. Phys.* **2010**, *49*, 060215.
[86] K. Fujiwara, T. Nemoto, M. J. Rozenberg, Y. Nakamura, H. Takagi, *Jpn. J. Appl. Phys.* **2008**, *47*, 6266.
[87] H. Shima, F. Takano, Y. Tamai, H. Akinaga, I. H. Inoue, *Jpn. J. Appl. Phys.* **2007**, *46*, L57.
[88] S. B. Lee, S. C. Chae, S. H. Chang, C. Liu, C. U. Jung, S. Seo, D.-W. Kim, *J. Korean Phys. Soc.* **2007**, *51*, S96.
[89] S. Zhang, S. Long, W. Guan, Q. Liu, Q. Wang, M. Liu, *J. Phys. D: Appl. Phys.* **2009**, *42*, 055112.
[90] Y. Taguchi, T. Matsumoto, Y. Tokura, *Phys. Rev. B* **2000**, *62*, 7015.
[91] S. Yamanouchi, Y. Taguchi, Y. Tokura, *Phys. Rev. Lett.* **1999**, *83*, 5555.
[92] R. Kumai, Y. Okimoto, Y. Tokura, *Science* **1999**, *284*, 1645.
[93] F. Sabeth, T. Iimori, N. Ohta, *J. Am. Chem. Soc.* **2012**, *134*, 6984.
[94] a) T. Oka, R. Arita, H. Aoki, *Phys. Rev. Lett.* **2003**, *91*, 066406; b) T. Oka, H. Aoki, *Phys. Rev. B* **2010**, *81*, 033103; c) T. Oka, H. Aoki, *Phys. Rev. Lett.* **2005**, *95*, 137601.
[95] F. Heidrich-Meisner, I. González, K. A. Al-Hassanieh, A. E. Feiguin, M. J. Rozenberg, E. Dagotto, *Phys. Rev. B* **2010**, *82*, 205110.
[96] M. Eckstein, T. Oka, P. Werner, *Phys. Rev. Lett.* **2010**, *105*, 146404.

[97] H. Aoki, N. Tsuji, M. Eckstein, M. Kollar, T. Oka, P. Werner, *Rev. Mod. Phys.* **2014**, *86*, 779.
[98] V. Dubost, T. Cren, C. Vaju, L. Cario, B. Corraze, E. Janod, F. Debontridder, D. Roditchev, *Adv. Funct. Mater.* **2009**, *19*, 2800.
[99] C. Vaju, L. Cario, B. Corraze, E. Janod, V. Dubost, T. Cren, D. Roditchev, D. Braithwaite, O. Chauvet, *Microelectron. Eng.* **2008**, *85*, 2430.
[100] The circuit used for resistive switching experiments is schematized in Figure 8a.
[101] M. E. Levinshtein, J. Kostamovaara, S. Vainshtein, Breakdown Phenomena in Semiconductors and Semiconductor Devices, *Selected Topics in Electronics and Systems, vol. 36*, World Scientific, Singapore **2005**.
[102] V. Guiot, L. Cario, E. Janod, B. Corraze, V. Ta Phuoc, M. Rozenberg, P. Stoliar, T. Cren, D. Roditchev, *Nat. Commun.* **2013**, *4*, 1722.
[103] J. L. Hudgins, G. S. Simin, E. Santi, M. A. Khan, *IEEE Trans. Power Electron.* **2003**, *18*, 907.
[104] J. L. Hudgins, *J. Electron. Mater.* **2003**, *32*, 471.
[105] H. Frohlich, *Proc. R. Soc. Lond. Ser. Math. Phys. Sci.* **1937**, *160*, 230.
[106] H. Frohlich, *Proc. R. Soc. Lond. Ser. Math. Phys. Sci.* **1947**, *188*, 521.
[107] F. Klappenberger, K. F. Renk, R. Summer, L. Keldysh, B. Rieder, W. Wegscheider, *Appl. Phys. Lett.* **2003**, *83*, 704.
[108] P. Stoliar, L. Cario, E. Janod, B. Corraze, C. Guillot-Deudon, S. Salmon-Bourmand, V. Guiot, J. Tranchant, M. Rozenberg, *Adv. Mater.* **2013**, *25*, 3222.
[109] P. Stoliar, M. Rozenberg, E. Janod, B. Corraze, J. Tranchant, L. Cario, *Phys. Rev. B* **2014**, *90*, 045146.
[110] B. Corraze, E. Janod, L. Cario, P. Moreau, L. Lajaunie, P. Stoliar, V. Guiot, V. Dubost, J. Tranchant, S. Salmon, M.-P. Besland, V. T. Phuoc, T. Cren, D. Roditchev, N. Stéphant, D. Troadec, M. Rozenberg, *Eur. Phys. J. Spec. Top.* **2013**, *222*, 1046.
[111] M. Querré, B. Corraze, E. Janod, M. P. Besland, J. Tranchant, M. Potel, S. Cordier, V. Bouquet, M. Guilloux-Viry, L. Cario, *Key Eng. Mater.* **2014**, *617*, 135.
[112] *International Technology Roadmap for Semiconductors* **2013**. www.itrs.net, in Emerging Research Devices and in Emerging Research Materials (accessed: June 2015).
[113] J. Tranchant, E. Janod, B. Corraze, P. Stoliar, M. Rozenberg, M.-P. Besland, L. Cario, in *Phys. Status Solidi A* **2014**, *212*, 239.
[114] A. Umantsev, *Phys. Nonlinear Phenom.* **2007**, *235*, 1.
[115] V. Dubost, T. Cren, C. Vaju, L. Cario, B. Corraze, E. Janod, F. Debontridder, D. Roditchev, *Nano Lett.* **2013**,*13*, 3648.
[116] C. Schindler, S. C. P. Thermadam, R. Waser, M. N. Kozicki, *IEEE Trans. Electron Devices* **2007**, *54*, 2762.
[117] A. Pirovano, A. Lacaita, A. Benvenuti, F. Pellizzer, R. Bez, *IEEE Trans. Electron Devices* **2004**, *51*, 452.
[118] S. Lupi, L. Baldassarre, B. Mansart, A. Perucchi, A. Barinov, P. Dudin, E. Papalazarou, F. Rodolakis, J.-P. Rueff, J.-P. Itié, S. Ravy, D. Nicoletti, P. Postorino, P. Hansmann, N. Parragh, A. Toschi, T. Saha-Dasgupta, O. K. Andersen, G. Sangiovanni, K. Held, M. Marsi, *Nat. Commun.* **2010**, *1*, 105.
[119] S. Populoh, P. Wzietek, R. Gohier, P. Metcalf, *Phys. Rev. B* **2011**, *84*, 075158.
[120] D. Fournier, M. Poirier, M. Castonguay, K. D. Truong, *Phys. Rev. Lett.* **2003**, *90*, 127002.
[121] M. de Souza, A. Brühl, C. Strack, B. Wolf, D. Schweitzer, M. Lang, *Phys. Rev. Lett.* **2007**, *99*, 037003.
[122] E. Souchier, M.-P. Besland, J. Tranchant, B. Corraze, P. Moreau, R. Retoux, C. Estournès, P. Mazoyer, L. Cario, E. Janod, *Thin Solid Films* **2013**, *533*, 54.
[123] J. Tranchant, A. Pellaroque, E. Janod, B. Angleraud, B. Corraze, L. Cario, M.-P. Besland, *J. Phys. D: Appl. Phys.* **2014**, *47*, 065309.
[124] E. Souchier, L. Cario, B. Corraze, P. Moreau, P. Mazoyer, C. Estounes, R. Retoux, E. Janod, M. P. Besland, *Phys. Status Solidi RRL* **2011**, *5*, 53.
[125] J. Tranchant, E. Janod, L. Cario, B. Corraze, E. Souchier, J.-L. Leclercq, P. Cremillieu, P. Moreau, M.-P. Besland, *Thin Solid Films* **2013**, *533*, 61.